



TECHNISCHE
UNIVERSITÄT
WIEN
VIENNA
UNIVERSITY OF
TECHNOLOGY

MASTERARBEIT

Determination of Love and Shida numbers from VLBI

ausgeführt am

Institut für Geodäsie und Geophysik
der Technischen Universität Wien

unter der Anleitung von

Univ.Prof. Dr. Ing. Harald Schuh
und

Univ.Ass. Dipl.-Ing. Dr. techn. Johannes Böhm
Dipl.-Ing. Dr. techn. Paulo Jorge Mendes Cerveira
als verantwortlich mitwirkenden Universitätsassistenten

durch

Hana Špičáková
E 066 463 / 0526728
Garnisongasse 14-16/501
A-1090 Wien

Acknowledgement

I would like to take this opportunity to express my big thanks to all, who helped me and supported me in writing this thesis.

Especially I want to express my gratitude to my principal supervisor, Prof. Harald Schuh, who gave me the possibility to stay at the Institute of Geodesy and Geophysics and to write this thesis there. His stimulating suggestions, comments and encouragement were guidelines of my work.

My sincere thanks belong to my co-advisors, Dr. Johannes Böhm and Dr. Paulo Mendes, for helping me at any time, introducing me into OCCAM software and giving me constant guidance and encouragement.

My special thanks go to Dipl.-Ing. Robert Heinkelmann for his interest and valuable hints.

Especially I am obliged to Dipl.-Ing. Andrea Pany, who has volunteered her time for looking closely at the final version of the thesis for English style and grammar, correcting both and offering suggestions for improvement.

I also want to express the acknowledgement to the “Mondi Austria Privatstiftung” for their financial support, which made my master study at TU Vienna possible.

Abstract

The Moon and Sun exert a gravitational force on the Earth. This influence in a certain point in the Earth or on the Earth's surface is a function of the distance between this point and the perturbing celestial bodies. The tidal attraction of the Moon or Sun in a certain point in the Earth is defined as the difference between the gravitational attraction in the point itself and the gravitational attraction in the geocentre. The tidal forces cause periodic deformations of the Earth's surface, and the Earth's response to the acting forces depends on Love and Shida numbers, which describe the elasticity of the Earth.

Modern space geodetic techniques, such as VLBI (Very Long Baseline Interferometry), allow the validation of theoretically estimated global Love and Shida parameters from direct measurements. The modelling of tidal displacement of the Earth's surface, as it is recommended in the IERS Conventions is implemented in the VLBI analysis software package OCCAM. In this thesis, a thorough description of the components of the tidal displacement is provided.

The main goal of this master thesis is to determine Love and Shida numbers of second degree obtained from observations during the CONT05 campaign, i.e. a 15 days continuous VLBI operation carried out in September 2005. Before applying the procedure for the determination of the Love numbers to real data, a Matlab-based program with simulated observations has been tested. When Earth rotation is considered, the Love numbers in the diurnal band become frequency dependent with a resonance around the frequency of the Free Core Nutation. In this thesis, the Love number h_2 , the Shida number l_2 , and Love numbers for six tidal waves (K_1 O_1 P_1 J_1 ψ_1 Φ_1) were estimated.

Table of Contents

| | |
|---|----|
| Acknowledgement | 2 |
| Abstract | 3 |
| Table of Contents | 4 |
| | |
| 1. Solid Earth tides | |
| 1.1 Introduction | 6 |
| 1.2 Tidal potential | 8 |
| 1.2.1 Harmonic expansion of tidal potential | 12 |
| (retaining only second degree) | |
| 1.2.2 Waves inside frequency bands | 15 |
| 1.3 Tidal displacement | 18 |
| 1.4 New definition in IERS Conventions 2003 | |
| 1.4.1 Theory of latitude dependent Love number parameters | 20 |
| 1.4.2 Computation procedure | 23 |
| | |
| 2. Free Core Nutation | 28 |
| | |
| 3. VLBI | |
| 3.1 Introduction | 30 |
| 3.2 Fundamental principle | 31 |
| 3.3 Phase delay versus group delay | 32 |
| 3.4 Sensitivity of the technique | 33 |
| 3.5 Signal detection and recording | 34 |
| 3.6 Signal correlation | 35 |
| 3.7 Data – CONT05 | 36 |
| 3.8 Software – OCCAM v.6 | 37 |

| | |
|---|----|
| 4. Analysis and Simulations | |
| 4.1 Total tidal displacement | 39 |
| 4.1.1 Tidal displacement at a station (15°E/50°N) | 40 |
| 4.1.2 Global tidal displacement | 43 |
| 4.2 Components of tidal displacement via IERS Conventions 2003 (contribution to radial displacement) | 46 |
| 4.3 Matlab simulation | 50 |
| 4.3.1 Input data | 51 |
| 4.3.2 Computation procedure | 52 |
| 4.3.3 Output values | 57 |
| 4.3.4 Influence of inexact h_2 on radial displacement | 59 |
| 4.4 Analysis in OCCAM | 60 |
| 4.4.1 Nominal values h_2 and l_2 | 61 |
| 4.4.2 Frequency dependent h_{21} for six diurnal waves | 65 |
| 5. Conclusions | 70 |
| References | 71 |

1. Solid Earth Tides

1.1 Introduction

Earth tides are caused by the gravitational attraction of the Moon and the Sun. The Moon, which orbits the Earth in an approximate distance of 384000 km, exerts a greater influence than does the Sun, being 150 million km away from the Earth.

When talking about tides, most people are referring to ocean tides (regular rise and decrease of ocean water) that can be observed at the ocean's coasts. However, not only the oceans but also the solid Earth is affected by the attracting forces of celestial bodies.

Nevertheless, the apparent ocean tides that are visible at the sea are the difference between the tidal displacements of the ocean and the solid Earth.

The vertical amplitude, which is caused by the pure solid Earth tides each day, can reach up to tens of centimetres.

Since an observer on the Earth's surface is following the upward and downward motions of the ground, the solid Earth tides are difficult to measure. Analogously, one is not able to take notice of ocean tides while standing in the middle of the ocean – our eyes must have a reference and see both, the ocean and the land.

Earth tides were already indirectly observed about one and half century ago. At that time a geological hypothesis existed that introduced the Earth with a molten interior upon which rests a relatively thin solid crust. This assumption was based on the extrapolation of the measured temperature gradient.

About 1863, Kelvin analysed observations of fortnightly tides, which were carried out in the Indian Ocean. From these observations it appeared that the observed amplitude was only about two-thirds of the theoretical one. In other words, the Earth's crust tides are three times lower as compared to the ocean tides. This historical result led to the statement that the rigidity of the Earth is about the same as that of steel (Love, 1927).

Augustus E.H. Love introduced a new radial parameter (h) describing spherical elasticity in 1909. In 1912, Shida added the tangential counterpart, i.e., l . These parameters are dimensionless numbers, which characterize the ability of the Earth to react elastically to tide-generating forces.

For brevity and according to other publications the term “Love numbers” includes both terms, i.e. h and l .

1.2 Tidal potential

The tidal potential (i.e. the tide generating potential, TGP) V^{tid} in a point P on the surface or within the Earth is the sum of the gravitational potential $V^{grav}(P)$ of the perturbing body (the Moon or the Sun) in the point P and of the potential of the centrifugal force $Q(P)$ due to the motion of the attracting body (the Moon or the Sun) around the barycentre of the two-body system.

$$V^{tid}(P) = V^{grav}(P) + Q(P) \quad (\text{E 1.1})$$

The tidal force (i.e. the gradient of the TGP) tends to deform the Earth, and this deformation is the Earth tide.

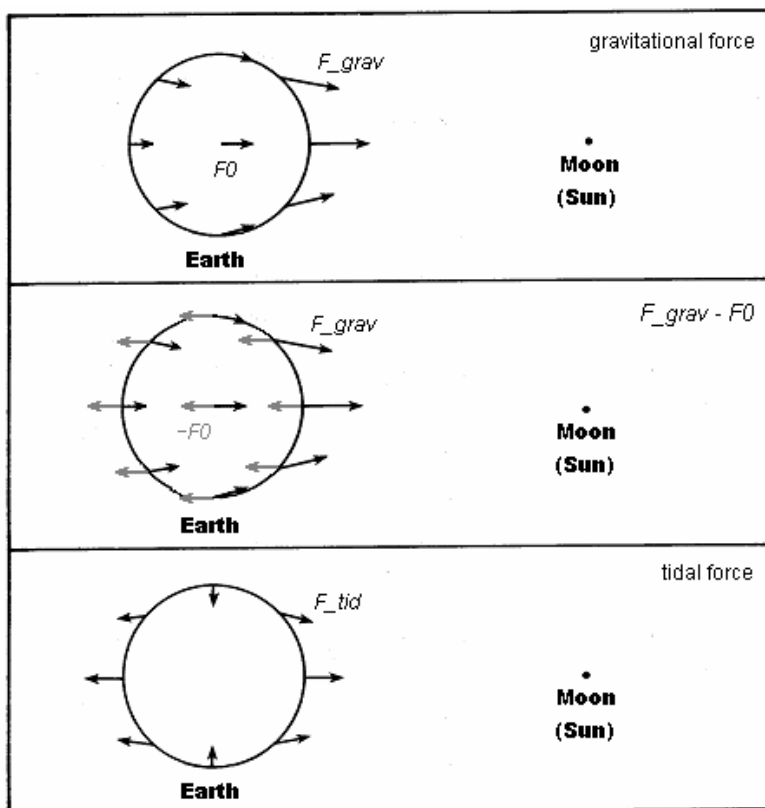


Figure (F 1.1): Gravitational force F_{grav} and tidal force F_{tid} acting on the Earth. Tidal force is obtained by subtracting the gravitational force vector acting in the geocentre F_0 from the F_{grav} . Modified from (Wahr, 1995).

From the upper part of Figure (F 1.1) it can be seen that the vectors of the gravitational force F_{grav} of the perturbing body on the Earth have unequal lengths and directions. The actual gravitational force depends on the distance of the perturbing body: the closer it is, the larger is the gravitational force.

The tidal force F_{tid} at the actual point in the Earth is obtained by subtracting the vector F_0 (i.e. gravitational force vector in the geocentre) from the gravitational force F_{grav} at point P (F 1.1 middle). The resulting tidal forces are illustrated in Figure (F 1.1 bottom).

Evidently, in the geocentre the tidal force equals zero. On the line, which connects the point underneath the perturbing body with the one on the antipode, the tidal forces are directed away from the centre of the Earth. At these sides, the Earth is deformed with two tidal bulges. On the perpendicular line (which is equivalent to the Earth's axis if the perturbing body is in equator plane) the tidal forces are directed to the geocentre and cause additional pole flattening.

Gravitational potential at point P caused by the Moon

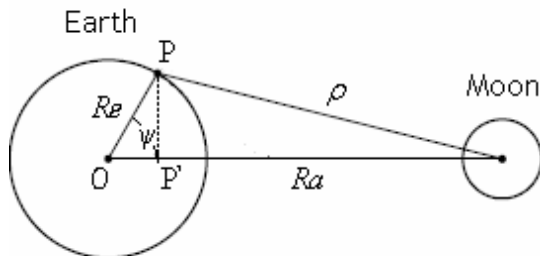


Figure (F 1.2): The basic geometry of the two bodies.

Because of the symmetry around the axis connecting the centres of the Earth and the perturbing body, the gravitational potential can be described with respect to this axis by

$$V^{grav} = \frac{GM_a}{\rho} \tag{E 1.2}$$

, where the topocentric distance ρ can be computed with the law of cosines (see Figure F 1.2)

$$\rho = R_e^2 + R_a^2 - 2R_e R_a \cos \psi \tag{E 1.3}$$

In Equation (E 1.3), R_a is the geocentric distance to the perturbing body, and R_e the geocentric distance to point P. Precise ephemerides allow us to compute the resulting tidal potential for a given point and instant, where the potential depends only on the geocentric zenith distance (ψ) of the perturbing body.

The following mathematical derivation for the tidal potential given by a sum of Legendre polynomials (E 1.8) is based on Zeman (2005).

The gravitational potential can be expressed as an expansion in Legendre polynomials (e.g. Burša and Kostelecký, 1999):

$$V^{grav} = \frac{GM_a}{R_a} \sum_{n=0}^{\infty} \left(\frac{R_e}{R_a} \right)^n P_n(\cos \psi) \quad (\text{E 1.4})$$

If the two-body system (the Earth – the Moon/Sun) should be in equilibrium, than the centrifugal force must be equal to the gravitational force from the perturbing body in the geocentre (O):

$$V^{tid}(O) = -Q(O) = \frac{GM_a}{R_a} \quad (\text{E 1.5})$$

As noticed earlier, the centrifugal acceleration in the whole Earth is constant. The equipotential surfaces of that centrifugal field are perpendicular to the line connecting the geocentre and the perturbing body. The difference in the centrifugal potentials between the geocentre (O) and the point (P) on the surface expresses Equation (E 1.6).

$$Q(P) - Q(O) = -\frac{GM_a}{R_a^2} \cdot |\text{OP}| = -\frac{GM_a}{R_a^2} \cdot R_e \cos \psi \quad (\text{E 1.6})$$

Deriving Equation (E 1.6) with respect to $|\text{OP}|$ yields a constant acceleration for the whole surface.

Introducing Equations (E 1.4), (E 1.5) and (E 1.6) in (E 1.1), the tidal potential becomes:

$$V^{tid} = V^{grav}(P) + Q(O) + (Q(P) - Q(O)) = \frac{GM_a}{R_a} \sum_{n=0}^{\infty} \left(\frac{R_e}{R_a} \right)^n P_n(\cos \psi) - \frac{GM_a}{R_a} - \frac{GM_a}{R_a^2} R_e \cos \psi \quad (\text{E 1.7})$$

The second and third term in (E 1.7) are identical to the first two terms of the gravitational potential (E 1.4) (i.e. the terms of zero and first degree in Legendre expansion). The final equation for the TGP is thus given by a sum of Legendre polynomials, which starts with degree two:

$$V^{tid} = \sum_{n=2}^{\infty} V_n = \frac{GM_a}{R_a} \sum_{n=2}^{\infty} \left(\frac{R_e}{R_a} \right)^n P_n(\cos \psi) \quad (\text{E 1.8})$$

Constraints of the tidal potential for practical computation

a) Which perturbing bodies do we need to consider?

If we look at the second degree tidal potential, $n = 2$, i.e.

$$V^{tid} = \frac{GM_a}{R_a} \cdot \left(\frac{R_e}{R_a}\right)^2 P_2(\cos\psi) , \text{ the magnitude of the potential is proportional to } \frac{GM_a}{R_a^3} .$$

In Table (T 1.1a) the values for Sun, Venus and Jupiter are shown relative to the value for the Moon.

| $\frac{GM_a}{R_a^3}$ | Moon | Sun | Venus | Jupiter |
|--------------------------------|-------------|------------|--------------|----------------|
| $\frac{GM_{Moon}}{R_{Moon}^3}$ | 1 | 0,46 | 0,000 05 | 0,000 006 |

Table (T 1.1a): Proportionality of the second degree tidal potential relative to the Moon’s value.

Even for the most precise computation it is sufficient to consider *only the lunisolar tides* (as recommended in the IERS Conventions 2003).

b) Up to which degree do we need to sum?

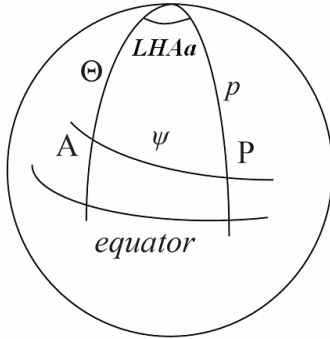
It is evident from $\left(\frac{R_e}{R_a}\right)^n$ that the importance of terms in the sum decreases fairly rapidly with increasing n .

| Perturbing body | $n = 2$ | $n = 3$ |
|---|---------------------------|----------------------------------|
| $\left(\frac{R_e}{R_{Moon}}\right)^n \cong \left(\frac{1}{60}\right)^n$ | $\frac{1}{3600}$ | $\frac{1}{216000}$ |
| $\left(\frac{R_e}{R_{Sun}}\right)^n \cong \left(\frac{1}{23000}\right)^n$ | $\frac{1}{529000000}$ | $\frac{1}{1.2167 \cdot 10^{13}}$ |

Table (T 1.1b): Importance of higher-degree Legendre polynomials decreases with increasing n .

Regarding values in Table (T 1.1b) and according to (McCarthy and Petit, 2004) *only second degree terms for the Sun and second and third degree terms for the Moon* need to be considered for precise computations.

For further theoretical considerations it is more interesting to express the angle ψ in geocentric coordinates (Θ, λ) of the station P and (p, GHA_a) of the attracting body A. The TGP can be described with respect to the Earth's axis of rotation, which is more useful than the description to the line connecting the mass centre of the Earth with the perturbing body.



- Θ colatitude of station
- λ longitude of station
- δ_a declination of the perturbing body
- $p = 90^\circ - \delta_a$ geocentric polar distance of the perturbing body
- GHA_a Greenwich hour angle
- $LHA_a = (GHA_a - \lambda)$ local hour angle of the perturbing body = angle between the meridian of the celestial object and the meridian of the observer

Figure (F 1.3): Geocentric coordinates of the station (P) and the Moon/Sun (A).

With the spherical law of cosines, the geocentric angle ψ can be expressed in geocentric spherical coordinates of the station P and the celestial body A (Figure F 1.3):

$$\cos\psi = \cos\Theta\cos p + \sin\Theta\sin p\cos(GHA_a - \lambda) \quad (\text{E 1.9})$$

Concerning spherical functions, the Legendre polynomials for ψ can be expressed with the addition theorem (E 1.10) (e.g. Burša and Kostelecký, 1999).

$$P_{n0}(\cos\psi) = P_{n0}(\cos\Theta) \cdot P_{n0}(\cos p) + \sum_{m=1}^n \frac{(n-m)!}{(n+m)!} P_{nm}(\cos\Theta) P_{nm}(\cos p) \cos m(GHA_a - \lambda) \quad (\text{E 1.10})$$

1.2.1 Harmonic expansion of the tidal potential (retaining only second degree)

Due to the periodically changing mutual positions between the point on the Earth's surface and the perturbing body, the tidal forces at the Earth's surface (and thus also the tidal deformation) occur in regular periods.

The time dependence of tidal waves is on one hand due to the rotation of the Earth, where the configuration "point P – perturbing body" is varying with a daily period. On the other hand, the frequency bands come from the periodical changes in the geocentric positions of the perturbing bodies. This is reflected in the geocentric declination δ_a , the Greenwich hour angle GHA_a and the geocentric distance R_a .

In order to describe the main frequency bands in the tidal perturbation separately, it is necessary to use spherical harmonics, where the tides can be split into three groups: long-periodic, diurnal, semidiurnal.

According to Equation (E 1.10) and retaining only the principal term $n = 2$, the expansion of the tide generating potential is introduced in Table (T 1.2). The tidal potential is expressed as a sum of spherical harmonics of degree 2 with coefficients representing the periodic functions of time.

Zonal part: $n = 2, m = 0$

The zonal part of the tidal potential V_{20}^{tid} is composed of a zonal harmonic for station colatitude $P_{20}(\cos \Theta)$ and a zonal harmonic for polar distance of the perturbing body $P_{20}(\cos p)$.

A zonal harmonic is a spherical harmonic of the form $P_{20}(\cos \vartheta)$, i.e. one, which reduces to a Legendre polynomial, where ϑ is Θ or p , respectively. Nodal lines on a unit sphere, where $P_{20}(\cos \vartheta)$ vanishes, are parallels of $\pm 35^{\circ} 16'$ latitude, which divide the surface into zones with different sign.

At a given time instant, $P_{20}(\cos \Theta)$ is constant for a parallel and $P_{20}(\cos p)$ is constant for the entire Earth. The geocentric declination of the Moon varies with time between $\pm 28^{\circ} 45'$ with a monthly period. The Sun's declination ranges from 23.5° to -23.5° with an annual period. Evidently, the value of $P_{20}(\cos p)$ stays always negative. The zonal part of the tidal potential field leads to the long-periodic tides.

Tesseral part: $n = 2, m = 1$

The tesseral spherical harmonics are the product of Legendre function $P_{21}(\cos \vartheta)$ and $\cos \Lambda$ (ϑ and Λ denote colatitude and longitude on a unit sphere). The tesseral harmonic function corresponds to a diurnal period. The curve on which they vanish are $n - m = 1$ parallel of latitude (it is the equator) and $2m = 2$ meridians (90° from the meridian of the perturbing body). Thus, the amplitudes at the equator and at the poles are permanently zero.

Sectorial part: $n = m = 2$

The product of Legendre function $P_{22}(\cos \vartheta)$ and $\cos 2\Lambda$ is termed sectorial spherical harmonic. It is actually a special case of the tesseral harmonics, where the degree n equals the order m . The sign does not change within $2m = 4$ longitude intervals, so the fundamental tidal period is semidiurnal.

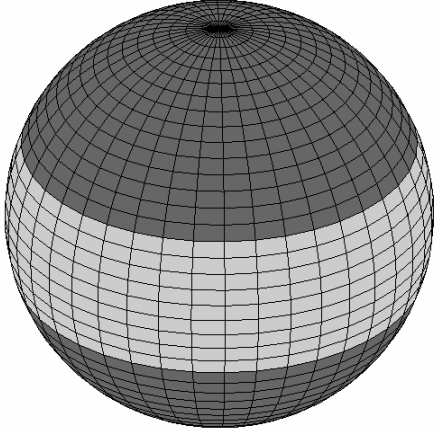
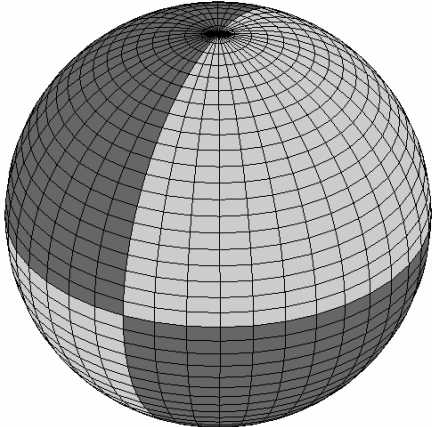
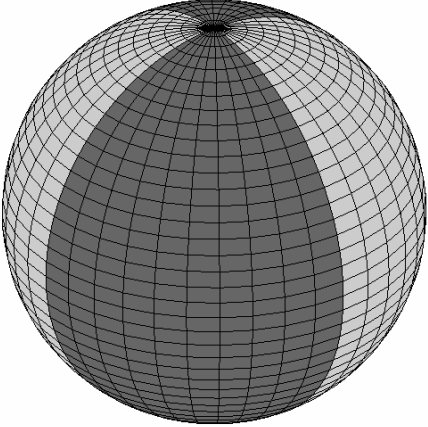
| | |
|---|---|
| $V_2^{tid} = \frac{GM_a}{R_a} \cdot \left(\frac{R_e}{R_a}\right)^2 P_2(\cos \psi) \quad (E 1.11)$ | |
| $V_2^{tid} = V_{20}^{tid} + V_{21}^{tid} + V_{22}^{tid} \quad (E 1.12)$ | |
|  <p>ZONAL HARMONIC</p> | $V_{20}^{tid} = GM_a \frac{R_e^2}{R_a^3} P_{20}(\cos \Theta) P_{20}(\cos p) \quad (E 1.13)$ <p>long period tides</p> <p>fundamental period 14 days for Moon 6 months for Sun (because of the squared sine function of the declination of the attracting body)</p> <p>does not depend on stations longitude</p> <p>zero value: latitude = $\sim 35^\circ$</p> |
|  <p>TESSERAL HARMONIC</p> | $V_{21}^{tid} = \frac{1}{3} GM_a \frac{R_e^2}{R_a^3} P_{21}(\cos \Theta) P_{21}(\cos p) \cos(GHA_a - \lambda) \quad (E 1.14)$ <p>diurnal tides</p> <p>a tesseral function divides sphere into areas, which change the sign once in latitude and twice in longitude</p> <p>zero value: latitude = $0^\circ, \pm 90^\circ$ declination = 0° ($GHA_a - \lambda$) = $\pm 90^\circ$</p> |
|  <p>SECTORIAL HARMONIC</p> | $V_{22}^{tid} = \frac{1}{12} GM_a \frac{R_e^2}{R_a^3} P_{22}(\cos \Theta) P_{22}(\cos p) \cos 2(GHA_a - \lambda) \quad (E 1.15)$ <p>semidiurnal tides</p> <p>the sign does not change within $2m = 4$ longitude intervals</p> <p>zero value: declination = $\pm 90^\circ$ for meridians = ($GHA_a - \lambda$) $\pm 45^\circ$</p> |

Table (T 1.2): Basic characteristics of the spherical harmonics of second degree.

1.2.2 Waves inside frequency bands

Inside the long-periodic, diurnal and semidiurnal frequency band a huge amount of specific tidal waves with own frequencies, which are slightly different from the frequency of the band, is hidden.

One reason for their existence is the variation of the inclination of the lunar orbit plane to the equator plane and of the inclination of the equator plane to the plane of the ecliptic. Secondly, it is caused by the ellipticity of the Moon's and the Earth's orbits.

To analyse the tidal phenomena, the components of these motions have to be separated in order to describe the tidal potential as a sum of waves having as argument linear functions of time. Doodson chose six variables that, when linearly combined, yield the argument of the specific tide.

Doodson's fundamental arguments

| | |
|--------------------|--|
| τ | mean lunar time |
| s | mean longitude of the Moon |
| h | mean longitude of the Sun |
| p | mean longitude of the lunar perigee |
| $N' = -N$ | mean longitude of the ascending lunar node which is changed in sign because of retrogression of the node |
| p_s | mean longitude of the perihelion |
| $t = \tau + s - h$ | mean solar time |

Systematic classification of tidal waves

In 1921, Doodson introduced a notation, which makes possible the automatic classification of all tidal waves, deduced from theory, in the order of their increasing speed. The parameter used, called the argument number (AN), can be deduced from mathematical expression of the argument of the tide (θ_f). The argument is a function of the six independent variables:

$$\theta_f = a\tau + bs + ch + dp + eN' + fp_s$$

The argument number is then obtained by the combination of six successive ciphers:

$$AN = a(b+5)(c+5)(d+5)(e+5)(f+5) = n_1n_2n_3 \cdot n_4n_5n_6$$

The first three variables have the greatest velocity. Thereby, the first three numbers are separated from the last three numbers by a dot.

| | Description | Separable after |
|-------------|--|-----------------------------------|
| n_1 | species number in the sense of Laplace 0 – long period wave 1 – diurnal wave 2 – semidiurnal wave ... | only a few days of observation |
| n_1n_2 | group number | one month of observation |
| $n_1n_2n_3$ | the constituent number | at least one year of observations |

Table (T 1.3): The first three digits of the argument number (Melchior, 1983).

The first digit of the argument number is precisely the species number in the sense of Laplace. It represents the types of spherical harmonic functions. There are three periods given for the spherical harmonics of the second order: long period ($n_1 = 0$), diurnal period ($n_1 = 1$), and semidiurnal period ($n_1 = 2$).

The first two digits of the argument number represent the group number, which characterizes the tidal waves separable from one month of observations.

This first section of three digits of the argument number is called the “constituent number”.

It differentiates the tidal waves, which we can separate considering that we have at least one-year of observations.

The last three indices ($n_4n_5n_6$) represent effects of a very slow variation. The waves whose arguments can only be distinguished in this part of the argument can only be separable if extensive continuous observations are available. (Melchior, 1983)

In this thesis, six diurnal components of tidal waves were selected for Matlab simulations (Chapter 4.3).

| Symbol | Argument number (AN) | Argument (θ_f) | Frequency [$^\circ/h$] | Amplitude | Origin (Lunar, Solar) | |
|----------|----------------------|-------------------------|--------------------------|-----------|-----------------------|--------------------------|
| O_1 | 145.555 | $\tau - s$ | 13.943036 | +37689 | L | principal lunar wave |
| P_1 | 163.555 | $t - h$ | 14.958931 | +17554 | S | solar principal wave |
| K_1 | 165.555 | $\tau + s$ | 15.041069 | -53050 | L+S | declinational wave |
| ψ_1 | 166.554 | $(t + h) + (h - p_s)$ | 15.082135 | -423 | S | elliptic wave of sK_1 |
| Φ_1 | 167.555 | $t + 3h$ | 15.123206 | -756 | S | declinational wave |
| J_1 | 175.455 | $(\tau + s) + (s - p)$ | 15.585443 | -2964 | L | elliptic wave of mK_1 |

Table (T 1.4): Tidal waves in the diurnal band with largest amplitudes and those lying close to the Nearly Diurnal Free Wobble resonance.

Conversion of tidal amplitudes defined according to different conventions

The definitions used for the amplitudes of tidal terms differ from each other and various definitions of amplitudes are given in literature.

The original definition from Doodson (1921) is dimensionless. The IERS Conventions 2003 (and the OCCAM source-code) follow the definition from Cartwright and Tayler (1971), where the tidal amplitude H_f is expressed as a height of tidal wave in meters. For completeness it should be mentioned, that Hartmann and Wenzel (1995) tabulated amplitudes in units of the potential [m^2s^{-2}].

| Factors for conversion to Cartwright-Tayler amplitudes H_f | |
|---|--|
| from Doodson | from Hartmann & Wenzel |
| $f_{20} = -\sqrt{\frac{4\pi}{5}} \frac{D_1}{g_e} = -0,426105$ | $f'_{20} = \frac{2\sqrt{\pi}}{g_e} = 0,361788$ |
| $f_{21} = -\frac{2}{3}\sqrt{\frac{24\pi}{5}} \frac{D_1}{g_e} = -0,695827$ | $f'_{21} = -\frac{\sqrt{8\pi}}{g_e} = -0,511646$ |
| $f_{22} = \frac{2}{3}\sqrt{\frac{24\pi}{5}} \frac{D_1}{g_e} = 0,695827$ | $f'_{22} = \frac{\sqrt{8\pi}}{g_e} = 0,511646$ |
| Doodson constant: $D_1 = 2,63358352855 \text{ m}^2 \text{ s}^{-2}$ | |
| g at the equatorial radius $g_e = 9,79828685 \text{ m s}^{-2}$ | |

Table (T 1.5): Conversion's amplitudes factors (McCarthy and Petit, 2004).

1.3 Tidal displacement

If the Earth was a perfectly rigid body, the tidal potential would only cause changes of the equipotential areas, e.g. changes in the Earth's gravitational potential. No transfer of masses or deformations of the crust would occur. The Earth is, however, not an ideally incompressible rigid body, so it does change its shape.

In 1909, Love introduced a new parameter h in his publication "The Yielding of the Earth to Disturbing forces". The parameter reflects the amount by which the surface of the Earth responds to the tide-generating forces.

It is a constant of proportionality between the radial tidal displacement of the Earth's crust $\delta\bar{\rho}$ and the radial tidal displacement of the equipotential surface $\delta\rho$. (Burša, 1988).

$$h = \frac{\delta\bar{\rho}}{\delta\rho} \quad (\text{E 1.16})$$

For a rigid body, $\delta\bar{\rho} = 0$, so the value of h is also equal to zero. For a perfectly fluid, $h = \frac{5}{2}$.

A parameter (l) for transverse displacement was introduced in 1912 by Shida and Lambert.

Considering the Earth being "Spherical, Non-Rotating, Elastic and Isotropic", what is the most basic model, the tidal displacement at a given station (Φ, λ) in the topocentric system (REN) is described by Equations (E 1.17 – E 1.19).

$$\text{Radial direction} \quad u_r = h \cdot \frac{1}{g} \cdot V^{tid} \quad (\text{E 1.17})$$

$$\text{East direction} \quad u_\lambda = l \cdot \frac{1}{g \cdot \cos\Phi} \cdot \frac{\partial V^{tid}}{\partial \lambda} \quad (\text{E 1.18})$$

$$\text{North direction} \quad u_\Phi = l \cdot \frac{1}{g} \cdot \frac{\partial V^{tid}}{\partial \Phi} \quad (\text{E 1.19})$$

Strictly speaking, in Equations (E 1.17 – E 1.19) the tidal potential is considered to be only of second degree. Consequently, the Love numbers h and l are constants at Earth's surface for

the second degree of the tide-generating potential. It needs to be mentioned, that each degree of the TGP has its own constant of proportionality. If higher degrees of TGP are added, the Love numbers for these terms appear. Simultaneously, the Love numbers are also functions of the geocentric distance.

So, the values $h_n(\rho) = h_2 = h$ and $l_n(\rho) = l_2 = l$ in (E 1.17 – E 1.19) refer to the Earth surface and to the most important term of second degree in the tide-generating potential.

When a more realistic model of the Earth is considered, i.e. the ellipticity, rotation and the elastic mantle – fluid core boundary are taken into account, the relationship between the TGP and the tidal displacement becomes more complicated. The displacement vector u is composed of deformational parts of specific harmonic degree, order and specific frequency inside the band. Hereby, also the Love numbers $h_{nm}(f)$ and $l_{nm}(f)$ become frequency dependent. Due to the different rotational axes of mantle and core, the Earth has a normal mode with an eigenfrequency in diurnal frequency band. These phenomena lead to a resonance (see Chapter 2: Free Core Nutation) and a strong frequency dependence for diurnal Love Numbers inside the diurnal tidal band.

Equations (E 1.20 – E 1.22) for individual tides were determined by Wahr (1981).

$$\text{Radial direction} \quad u_r = \frac{1}{g} \cdot \sum_{n=2}^{n_{\max}} \sum_{m=0}^n \sum_T h_{nm}(f) \cdot V_{nmT}^{tid} \quad (\text{E 1.20})$$

$$\text{East direction} \quad u_\lambda = \frac{1}{g \cdot \cos \Phi} \cdot \sum_{n=2}^{n_{\max}} \sum_{m=0}^n \sum_T l_{nm}(f) \cdot \frac{\partial V_{nmT}^{tid}}{\partial \lambda} \quad (\text{E 1.21})$$

$$\text{North direction} \quad u_\Phi = \frac{1}{g} \cdot \sum_{n=2}^{n_{\max}} \sum_{m=0}^n \sum_T l_{nm}(f) \cdot \frac{\partial V_{nmT}^{tid}}{\partial \Phi} \quad (\text{E 1.22})$$

Further, for a more precise treatment, the anelasticity of the Earth's mantle can be put into a model, which causes a lag of the tidal deformation with respect to the TGP. Mathematically it is described by imaginary parts of the tidal displacement, if it is written as a complex function.

According to (Mathews, 1997), the mantle anelasticity causes displacements up to a few millimetres.

1.4 New definition in IERS Conventions 2003

1.4.1 Theory of latitude dependent Love number parameters

A completely new approach in definition of the Love numbers was introduced by Mathews et al. (1995).

“For an oceanless, elastic, spheroidal, rotating and nutating Earth, we present new definitions for the latitude dependent Love numbers and gravimetric constant which are free of certain drawbacks of the definitions currently in use, and make the computation of quantities of observational interest simpler and more direct.” (Mathews et al., 1995).

(Mathews et al, 1995) defined sets of parameters, which are used for the representation of the latitude dependence of the effective Love numbers h and l .

These parameters $h^{(0)}, h^{(2)}, h'$ and $l^{(0)}, l^{(1)}, l^{(2)}, l'$ are defined by their contribution to the site displacement due to a spectral component, which belongs to one of the three frequency bands (long period, diurnal, semidiurnal) of the tide generating potential (E 1.13 – E 1.15).

The values of these parameters, which are relevant for the computational procedure, are listed in Table 7.4 in the IERS Conventions 2003 (McCarthy and Petit, 2004).

The model of the solid Earth tides recommended in the IERS Conventions 2003 is based on this new definition.

| Dependence of the effective Love number parameters (McCarthy and Petit, 2004) | |
|---|---|
| | caused by |
| latitude dependence + small interband variations | Earth's ellipticity |
| | Coriolis force due to Earth rotation |
| frequency dependence | |
| - within the diurnal band | very strong, produced by the Nearly Diurnal Free Wobble resonance (NDFW), associated with FCN (see Chapter 2) |
| - within the long-period band | from mantle anelasticity |

Table (T 1.6): Causes of the latitude and frequency dependence of the effective Love numbers parameters.

The following expressions (E 1.23 – E 1.25) result from the evaluation of the defining equation “(6)” in Mathews et al. (1995).

Each frequency band has its own formula, where the frequency f has to be replaced by specific tide frequency inside the band.

Long period tide of frequency f is expressed as following

$$\Delta \vec{r}_f = \sqrt{\frac{5}{4\pi}} H_f \left\{ \begin{array}{l} \left[h(\Phi) \left(\frac{3}{2} \sin^2 \Phi - \frac{1}{2} \right) + \sqrt{\frac{4\pi}{5}} h' \right] \cos \theta_f \hat{r} + \\ + 3l(\Phi) \sin \Phi \cos \Phi \cos \theta_f \hat{n} + \\ + \cos \Phi \left[3l^{(1)} \sin^2 \Phi - \sqrt{\frac{4\pi}{5}} l' \right] \sin \theta_f \hat{e} \end{array} \right\} \quad (\text{E 1.23})$$

diurnal tide of frequency f is defined as

$$\Delta \vec{r}_f = -\sqrt{\frac{5}{24\pi}} H_f \left\{ \begin{array}{l} h(\Phi) 3 \sin \Phi \cos \Phi \sin(\theta_f + \lambda) \hat{r} + \\ + \left[3l(\Phi) \cos 2\Phi - 3l^{(1)} \sin^2 \Phi + \sqrt{\frac{24\pi}{5}} l' \right] \sin(\theta_f + \lambda) \hat{n} + \\ + \left[\left(3l(\Phi) - \sqrt{\frac{24\pi}{5}} l' \right) \sin \Phi - 3l^{(1)} \sin \Phi \cos 2\Phi \right] \cos(\theta_f + \lambda) \hat{e} \end{array} \right\} \quad (\text{E 1.24})$$

while semidiurnal tide of frequency f reads

$$\Delta \vec{r}_f = \sqrt{\frac{5}{96\pi}} H_f \left\{ \begin{array}{l} h(\Phi) 3 \cos^2 \Phi \cos(\theta_f + 2\lambda) \hat{r} - \\ - 6 \sin \Phi \cos \Phi [l(\Phi) + l^{(1)}] \cos(\theta_f + 2\lambda) \hat{n} - \\ - 6 \cos \Phi [l(\Phi) + l^{(1)} \sin^2 \Phi] \sin(\theta_f + 2\lambda) \hat{e} \end{array} \right\} \quad (\text{E 1.25})$$

where

$$h(\Phi) = h^{(0)} + h^{(2)} \left(\frac{3}{2} \sin^2 \Phi - \frac{1}{2} \right) \quad (\text{E 1.26})$$

$$l(\Phi) = l^{(0)} + l^{(2)} \left(\frac{3}{2} \sin^2 \Phi - \frac{1}{2} \right) \quad (\text{E 1.27})$$

| | |
|------------|---|
| H_f [m] | amplitude of the tidal term of frequency f (definition according to Cartwright and Tayler) |
| Φ | latitude of station |
| λ | east longitude of station |
| θ_f | tide argument for tidal constituent with frequency f |
| \hat{r} | unit vector in the radial direction |
| \hat{e} | unit vector in the east direction |
| \hat{n} | unit vector in the northward direction |

Note:

The contributions to the Love number parameters from anelasticity and ocean tidal loading as well as those from the centrifugal perturbations due to the wobbles have imaginary parts. These imaginary parts cause that the tidal displacement is slightly shifted from the tide generating potential (McCarthy and Petit, 2004). Generalization to the complex parameters can be done by making the following replacements:

$$\begin{aligned}
 L \cos(\theta_f + m\lambda) &\rightarrow L^R \cos(\theta_f + m\lambda) - L^I \sin(\theta_f + m\lambda) \\
 L \sin(\theta_f + m\lambda) &\rightarrow L^R \sin(\theta_f + m\lambda) + L^I \cos(\theta_f + m\lambda)
 \end{aligned}
 \tag{7a,b IERS}$$

where L is a generic symbol for $h^{(0)}, h^{(2)}, h', l^{(0)}, l^{(1)}, l^{(2)}, l'$.

Approximate maximum amplitude of the various contributions

| Description | Radial displacement (in phase) [mm] | Transverse displacement (in phase) [mm] |
|--------------------------------------|--|--|
| full degree 2 tide | 314 | 65 |
| full degree 3 tide | 1.7 | 0.2 |
| degree 2 zonal tide | 157 | 33 |
| permanent tide | 120 | 25 |
| degree 2 diurnal tide | 189 | 53 |
| degree 2 semidiurnal tide | 235 | 65 |
| Latitude dependence effect: degree 2 | | |
| $l^{(1)}$ term in semidiurnal tide | --- | 1.0 |
| $l^{(1)}$ term in diurnal tide | --- | 0.8 |
| $h^{(2)}$ and $l^{(2)}$ terms | 0.4 | 0.1 |

Table (T 1.7): Maximum amplitudes of the main contributions to the site displacement (Mathews et al., 1997).

Table (T 1.8) shows the contribution of the latitude dependence to the nominal values h_2 and l_2 of Love numbers. The defining equations are (E 1.26) and (E 1.27).

$$\begin{aligned}
 h^{(0)} = h_{22} &= 0.6078 & h^{(2)} &= -0.0006 \\
 l^{(0)} = l_{22} &= 0.0847 & l^{(2)} &= 0.0002
 \end{aligned}$$

| Φ | 0° | $\pm 30^\circ$ | $\pm 60^\circ$ | $\pm 90^\circ$ |
|--------------------------------|-----------------|-----------------|-----------------|-----------------|
| $h^{(2)} \cdot P_2(\sin \Phi)$ | 0.000 30 | 0.000 08 | -0.000 38 | -0.000 60 |
| h_2 | 0.607 8 | | | |
| $h(\Phi)$ | 0.608 10 | 0.607 88 | 0.607 42 | 0.607 20 |
| $l^{(2)} \cdot P_2(\sin \Phi)$ | -0.000 10 | 0.000 00 | 0.000 13 | 0.000 20 |
| l_2 | 0.084 7 | | | |
| $l(\Phi)$ | 0.084 60 | 0.084 70 | 0.084 83 | 0.084 90 |

Table (T 1.8): Contribution of the latitude dependence to the nominal Love numbers h_2 , l_2 .

1.4.2 Computation procedure

For practical use, it is very inefficient to compute the tidal deformation with a simple summation of Equations (E 1.23 – E 1.25) over the spectral components. This computation would lead to a large number of terms, which have to be considered in order to achieve an accuracy of 1 mm or better. Nevertheless, from a theoretical point of view it would be possible.

A more efficient computation of the variation of the station coordinates due to solid Earth tides is done by the use of a two-step-procedure, which was adopted in the IERS Conventions 2003. This procedure is also implemented in the VLBI data analysis software OCCAM, which is used at TU Vienna, and with which the computations for this master thesis were performed. The components of the tidal displacement from this procedure are visualised in Chapter 4.2 of his work.

IERS Conventions 2003
Chapter 7.1.2: Effects of the solid Earth Tides

| Step 1 Corrections in the time domain | | |
|---|---------------------------------------|-------------------------|
| S1.a | in-phase | |
| | S1.a.1 | for degree 2 tides |
| | S1.a.2 | for degree 3 tides |
| S1.b | out-of-phase only for degree 2 | |
| | S1.b.1 | diurnal |
| | S1.b.2 | semidiurnal |
| S1.c | contribution from latitude dependence | |
| | S1.c.1 | diurnal |
| | S1.c.2 | semidiurnal |
| Step 2 Corrections in the frequency domain for degree 2 | | |
| S2.a | semidiurnal tides | negligible |
| S2.b | diurnal tides | in phase corrections |
| S2.c | long period tides | in phase + out of phase |

Table (T 1.9): Two-step-procedure adopted in the IERS Conventions 2003 to computation of station coordinates variation due to solid Earth tides.

Step 1

▪ **S1.a.1 Displacement due to degree 2 tides**

Values of Love numbers for semidiurnal tides $h_{22}^{(0)}$ and $l_{22}^{(0)}$ are chosen to be nominal values for all degree 2 tides. The Love numbers have negligible variation in the semidiurnal band. Thus, the computational effort in Step 2 – correction in the frequency domain – is minimized.

$$h_{22}^{(0)} = 0.6078$$

$$l_{22}^{(0)} = 0.0847$$

Equation (E 1.28) is the initial equation “(9)” in the IERS Conventions 2003 (McCarthy and Petit, 2004), p.79, for the degree-2 tide. It corresponds to the basic equation of tide generating potential, which was introduced in Chapter 1 (E 1.11) with the displacement given by (E 1.17 – E 1.19).

$$u = \sum_{a=2}^3 \frac{GM_a R_e^4}{GM_e R_a^3} \left\{ h_2 \cdot \left(\frac{3}{2} (\hat{R}_a \cdot \hat{r})^2 - \frac{1}{2} \right) \hat{r} + 3l_2 (\hat{R}_a \cdot \hat{r}) \left[\hat{R}_a - (\hat{R}_a \cdot \hat{r}) \hat{r} \right] \right\} \quad (\text{E 1.28})$$

Conversion of Equation (E 1.17) into the radial part of Equation (E 1.28) is demonstrated in (E 1.29):

$$\begin{aligned}
 u_r &= h_2 \cdot \frac{V_2^{tid}}{g} = h_2 \cdot \frac{1}{g} \cdot \frac{GM_a}{R_a} \left(\frac{R_e}{R_a} \right)^2 P_2(\cos \psi) = h_2 \cdot \frac{R_e^2}{GM_e} \cdot \frac{GM_a}{R_a} \left(\frac{R_e}{R_a} \right)^2 P_2(\cos \psi) = \\
 &= \frac{GM_a R_e^4}{GM_e R_a^3} h_2 \cdot P_2(\cos \psi) = \frac{GM_a R_e^4}{GM_e R_a^3} h_2 \cdot \left(\frac{3}{2} (\hat{R}_a \cdot \hat{r})^2 - \frac{1}{2} \right)
 \end{aligned}
 \tag{E 1.29}$$

Separation of the transverse displacement into the eastward and the northward direction can be found e.g. in Sovers (1998):

$$u_{\lambda,2} = l_2 \cdot \sum_a \frac{3\mu_a R_e^3}{R_a^5} (\mathbf{R}_e \cdot \mathbf{R}_a) \frac{(x_s Y_a - y_s X_a)}{\sqrt{x_s^2 + y_s^2}}
 \tag{E 1.30}$$

$$u_{\phi,2} = l_2 \cdot \sum_a \frac{3\mu_a R_e^2}{R_a^5} (\mathbf{R}_e \cdot \mathbf{R}_a) \left[\sqrt{x_s^2 + y_s^2} Z_a - \frac{z_s}{\sqrt{x_s^2 + y_s^2}} (x_s X_a + y_s Y_a) \right]
 \tag{E 1.31}$$

- with
- X_a, Y_a, Z_a geocentric coordinates of the perturbing body
 - x_s, y_s, z_s geocentric coordinates of the station P
 - μ_a ratio of the mass of the perturbing body to the mass of the Earth
 - \mathbf{R}_e vector from the geocentre to the station P
 - \mathbf{R}_a vector from the geocentre to the Moon/Sun

Equation (E 1.32) defines radial displacement (Sovers,1998) and is identical with (E 1.28).

$$u_{r,2} = h_2 \cdot \sum_a \frac{3\mu_a R_e^2}{R_a^5} \left[\frac{(\mathbf{R}_e \cdot \mathbf{R}_a)^2}{2} - \frac{R_e^2 R_a^2}{6} \right]
 \tag{E 1.32}$$

(Equations E 1.30 – E 1.32 were used for partial derivatives in my source-code. See chapters (Ch 4.3.2) and (Ch 4.4)).

▪ **S1.a.2 Displacement due to degree 3 tides**

h_3, l_3 are taken to be real and constant. Only the Moon's contribution needs to be computed. Radial displacement can reach 1.7 mm, transverse displacement stays lower than 0.2 mm.

▪ **S1.b Out of phase contributions from imaginary parts of $h_{2m}^{(0)I}$ and $l_{2m}^{(0)I}$**

The contributions to radial and transverse displacements are computed with nominal values for the whole band (diurnal, semidiurnal). Corrections to this simplification are made in Step 2. For zonal tides, there is no closed expression in the time domain.

▪ **S1.c Contributions to the transverse displacement induced by latitude dependence**

| band | nominal $l^{(1)}$ real value | contribution to the transverse displacement |
|-------------|------------------------------|---|
| zonal | 0 | 0 |
| diurnal | 0.0012 | 0.8 mm |
| semidiurnal | 0.0024 | 1.0 mm |

Table (T 1.10): Contributions to the transverse displacement from the real part of the nominal value $l^{(1)}$.

The imaginary part of $l^{(1)}$ and the intraband variations of the real part are completely ignorable.

Step 2

Corrections to the radial and transverse station displacement caused by the intraband variations of degree 2 Love numbers are taken into account here.

In the diurnal band the frequency variation is caused by the NDFW resonance. The list of 11 constituents from the diurnal band with radial correction 0.05 mm or more, is given in Table 7.5a in the IERS Conventions 2003 (McCarthy and Petit, 2004)).

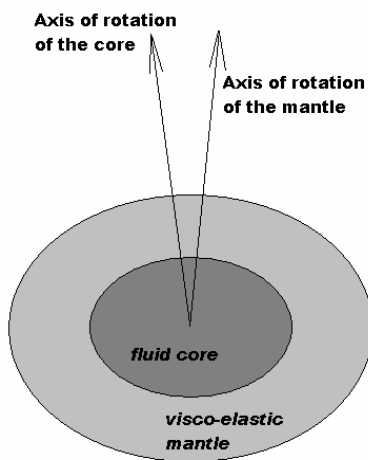
In the long period band, the Love numbers frequency dependence is due to the variation of the anelasticity contribution. According to Table 7.5b in IERS Conventions 2003 (McCarthy and Petit, 2004), the contributions of 5 terms with a radial correction of more than 0.05 mm need to be considered.

Corrections due to all constituents listed in (Tables 7.5a and 7.5b, IERS2003) must be taken into account to ensure an accuracy of 1 mm (McCarthy and Petit, 2004).

Nevertheless, in Mathews et al. (1997), it is stated, that variations of the imaginary parts are significant only in the long period band. In the diurnal band the only component that achieves the cutoff of 0.05 mm is due to the K_1 tide.

2. Free Core Nutation

The strong frequency dependence in the diurnal tidal response of the solid Earth is caused by inhomogeneities in the Earth's interior.



This variation of Love numbers with frequency in the diurnal band arises from resonance behaviour of the Earth, which is caused by the presence of the fluid core. The rotational axis of the core is slightly inclined with respect to the axis of rotation of the mantle. In this situation forces arise at the elliptical core-mantle boundary (CMB), which try to realign the two axes.

Figure (F 2.1): Axes of rotation of the fluid core and mantle.

In the terrestrial reference frame, this phenomenon is seen as a diurnal motion, and is called the Nearly Diurnal Free Wobble (NDFW). In the celestial reference frame it appears as a retrograde motion of the celestial pole with a period of approximately 430 days and is designated as Free Core Nutation (FCN).

With Very Long Baseline Interferometry the motion of the rotational axis of the mantle in celestial frame can be observed. Because any displacement of the core axis induces a displacement of the mantle axis, the FCN period can be determined from VLBI data analyses. The resonance period of FCN in space is dominated by the shape of the core. The period is inversely proportional to its dynamical flattening. If the core was in hydrostatic equilibrium, the period would be approximately 460 days – value used by (Wahr, 1981).

The later analyses of VLBI data show, that the core's flattening has to be slightly larger, because the estimated FCN period is around 430 solar days.

One of the most recent estimations of FCN period can be found in Vondrák and Ron (2006). Using data from April 1982 to June 2005, they estimated the FCN period to be equal to 430.55 ± 0.11 solar days (Vondrák and Ron, 2006).

The estimation of the FCN period from the tidal displacement was published, e.g., in Haas and Schuh (1996). For the estimation of the FCN period they used a resonance formula for the Love numbers in the diurnal tidal band, which was published by Wahr (1981):

$$h_{21}(f) = h_{21}(O_1) + h_{RS} \cdot \frac{\omega_f - \omega_{O_1}}{\omega_{FCN} - \omega_f} \quad (\text{E 2.1})$$

$$l_{21}(f) = l_{21}(O_1) + l_{RS} \cdot \frac{\omega_f - \omega_{O_1}}{\omega_{FCN} - \omega_f} \quad (\text{E 2.2})$$

$h_{21}(f), l_{21}(f)$ Love number of a tide T from diurnal band
 $\omega_f, \omega_{O_1}, \omega_{FCN}$ frequencies of each specific tide
 h_{RS}, l_{RS} resonance strength factor

It was solved for all five parameters: $h_{21}(f), l_{21}(f), h_{RS}, l_{RS}, \omega_{FCN}$. Because Equations (E 2.1) and (E 2.2) are not linear with respect to ω_{FCN} , iterations had to be carried out.

The period determined by Haas and Schuh (1996) from about 725000 VLBI observables (1979 – 1995) is 426 ± 20 sidereal days.

Equation (E 2.1) was used in the Matlab simulations for the determination of the NDFW frequency (see section Analysis and Simulations (Chapter 4.3)).

3. VLBI (Very Long Baseline Interferometry)

3.1 Introduction

The geodetic interest in VLBI is based on the use of an inertial frame formed by a given set of extremely compact extragalactic radio sources (quasars).

A Quasar (abbreviation of QUASi-stellar radio source) is an extremely bright and compact active galactic nucleus, which doesn't have measurable proper motions.

VLBI is the only technique that can link the terrestrial reference frame (TRF) and the quasi-inertial reference frame realized by positions of the radio sources. Due to this connection, VLBI is the unique technique for direct measurement of Earth orientation without hypotheses of all components.

VLBI provides Earth orientation data, which are affected by the Earth's response to numerous forces. These data can be used to extract characteristics of the oceans, atmosphere and solid Earth.

The main geodynamical phenomena such as polar motion, Universal Time (UT1), nutation and precession, Earth tides or tectonic plate motion are monitored via this technique with very high accuracy.

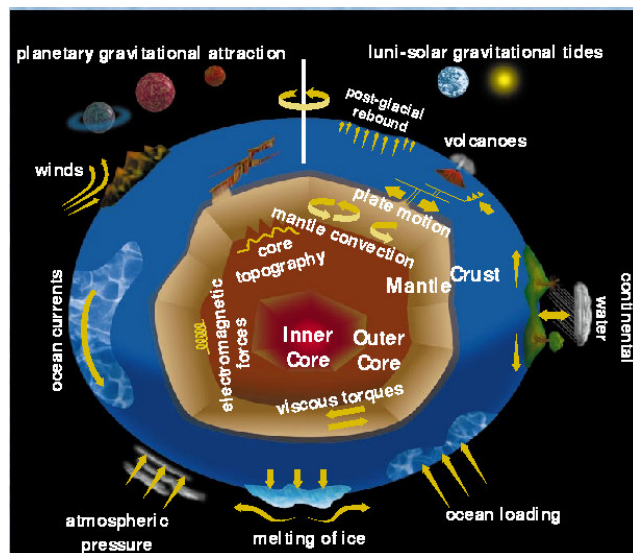


Figure (F 3.1): Numerous phenomena affect the orientation of the Earth. (Original drawing by Jos Verheijen, <http://lupus.gsfc.nasa.gov/brochure/bfuture2.html>).

Through constant improvements in the quality of the observations and their analyses, geodetic VLBI results have steadily been improved. Currently, the time difference measurements are precise to a few picoseconds. This means, that VLBI determines the relative positions of the antennas and the quasar positions with an accuracy of a few millimetres and fractions of a milliarcsecond, respectively. The precision that can be achieved in the VLBI products is summarized in the following table.

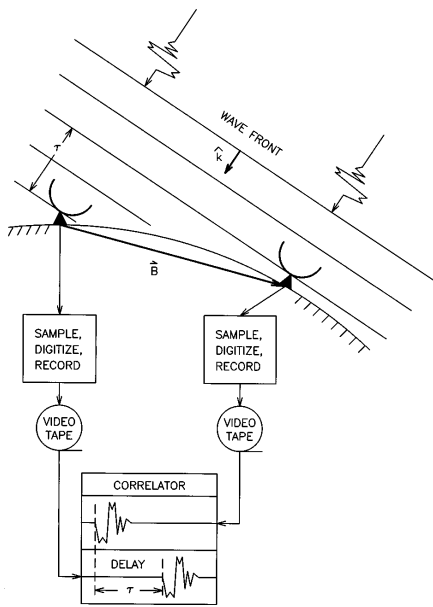
| Summary of current IVS main data products | | | |
|---|---|--------------------------|--------------------------------------|
| IVS Data Product | | Status 2002 | Goals (~2010) |
| CRF | α, δ | 0.25 – 3 mas | 0.25 mas + improved sky distribution |
| EOP | $\Delta\varepsilon, \Delta\psi$ | 100 – 400 μas | 25 – 50 μas |
| | UT1 from 24h session | 5 μs | 2 – 3 μs |
| | x_p, y_p | 200, 100 μas | 25 – 50 μas |
| TRF | x, y, z annual solution | 1 – 4 mm | 1 – 2 mm |
| | $\dot{x}, \dot{y}, \dot{z}$ annual solution | 0.1 – 1 mm/y | 0.1 – 0.3 mm/y |
| | x, y, z one solution per session | 5 – 20 mm | 2 – 5 mm |
| | | | |
| Solid Earth tides | h, l | 5 – 10% | 0.1% |

Table (T 3.1): IVS main data products, Final report of IVS Working Group 2 on data analysis (Schuh et al., 2002).

Following Chapters (Ch 3.2 – Ch 3.6) are based primarily on Campbell et al. (1992) and Campbell (2004).

3.2 Fundamental principle

The fundamental principle of geodetic VLBI is a synchronized observation of an extragalactic radio source. VLBI measures the time difference between the arrivals of a radio wavefront emitted by a quasar at two Earth-based antennas. This time delay τ , which is the principal observable in VLBI, is proportional to the scalar product of the baseline vector b between the two telescopes and the unit signal propagation vector k .



$$\tau = -\frac{1}{c}bk \tag{E 3.1}$$

c is the velocity of light. The negative sign is due to the conventions in defining τ and b .

Figure (F 3.2): Fundamental principle of geodetic VLBI measurement (Sovers, 1998).

One VLBI observation lasts a few minutes. The sources are observed at two frequency bands (X- and S-band) with frequencies of about 8.4 GHz (wavelength ~ 3.6 cm) and 2.3 GHz (wavelength ~ 13 cm), respectively. The observation at two frequency bands allows to correct for the ionospheric delay which is dependent on the frequency of the signal.

3.3 Phase delay or group delay

Despite the fact, that phase measurements are more precise than measurements of group delay, the prime geodetic VLBI observable is the wide band group delay of the quasar's signals.

The challenge with the phase measurement is the determination of ambiguities. For the observed frequency with a wavelength of 3.6 cm, the a priori geometry has to be known with an accuracy of better than 2 cm. For baselines with lengths of several thousands of kilometres, this is still a hard constraint. (Campbell et al., 1992)

The phase reference gets lost by the transition to another source. The antenna changes observing angle in the range of many degrees and begins to observe the second source with an unknown phase value. The connection to previous measurement is lost.

Phase delay is still an issue of research and does not provide very high accuracy on very short baselines.

In the early seventies, the Haystack Observatory in the north of Massachusetts and the National Radio Astronomy Observatory of Greenbank, West Virginia, conducted the first VLBI experiments that were explicitly aimed at achieving geodetic accuracy on long baselines. (Campbell, 2004)

To attain high resolution group delay measurements, it is necessary to record at bandwidths as broad as possible. Until that time, the registration was restricted through limited tape recording systems, which only allowed recording of a maximum 2 MHz band. In these experiments the so-called bandwidth synthesis technique was invented, which helped to overcome the limitations of data recording. The principle is, that the time delay is not derived from the whole frequency band, but only from the signals at the outer ranges of the band. To avoid the ambiguity problem, fixed-frequency channels are also recorded across the spanned bandwidth. The a priori station positions need to be known with an accuracy of a few meters. (Campbell et al., 1992)

3.4 Sensitivity of the technique

The signal to noise ratio (SNR) in interference time is given by

$$\text{SNR} = \eta \frac{F_d}{2k} \cdot \sqrt{\frac{A_1 \cdot A_2}{T_{S1} \cdot T_{S2}}} \cdot \sqrt{2BT} \quad (\text{E 3.2})$$

- η digital processing loss factor
- F_d signal flux density (1 Jansky = 10^{-26} W m⁻² Hz⁻¹)
- k Boltzmann's constant ($1.38 \cdot 10^{-23}$ m² kg s⁻² K⁻¹)
- A_1, A_2 effective antenna areas
- T_{S1}, T_{S2} noise temperatures of the receiver system
- B bandwidth of the recording system
- T coherent integration time

In Equation (E 3.2) it can be seen, that the SNR depends on the product of effective antenna areas. If a smaller antenna is used in combination with a large antenna, the resulting effect (in terms of SNR) is the same, as if two medium large antennas would be used.

The standard deviation σ_τ in the estimate of the group delay derived from bandwidth synthesis is proportional to the SNR and the spanned bandwidth B_{eff} :

$$\sigma_\tau = \frac{1}{2\pi \cdot \text{SNR} \cdot B_{eff}} \quad (\text{E 3.3})$$

The effective bandwidth is defined as the root mean square (rms) frequency deviation about the mean of the observed frequencies.

$$B_{eff} = \sqrt{\frac{\sum (f_i - f_m)^2}{N}} \quad (\text{E 3.4})$$

3.5 Signal detection and signal recording

The main part of a radiotelescope is a movable reflector with a feed horn. There are two possible ways of leading the signal to this horn. For a prime focus antenna, the signal goes directly from the paraboloidal reflector to the feed horn at the focus position. The second types of telescopes have an additional hyperboloidal subreflector. The incoming signal first strikes the paraboloidal dish of the antenna, is then reflected up to the subreflector, and finally enters the feed horn on the central axis.

To avoid a possible degradation of the signal, the initial stage of its amplification is done right under the feed horn. After the first stage of amplification, the signal is heterodyned from radio frequency to a lower intermediate frequency of around 300 MHz with a bandwidth of 400 MHz.

In a control building, the signal is split in several channels and further heterodyned into basic bands limited with frequencies between 0 and 2 MHz.

The dividing into the channels is performed to get, after a synthesis of all bands, a bandwidth as broad as possible. The width of the final band is essential for the precision in estimation of the time differences τ .

In the next step, the signal is digitized and marked with time stamps. Time and frequency information are provided by a Hydrogen maser (Microwave Amplification by Stimulated Emission of Radiation). The current stability of the H-maser supports the accuracy of the observable from 20 to 30 ps (the stability of the frequency standard is 1 part in 10^{14} over many hours of operation).

Finally, the data are recorded on high-capacity transportable hard disks and shipped to correlators.

3.6 Signal correlation

Correlators are facilities, in which the signals of two stations are combined. They consist of special-purposed signal processing hardware, that is used to determine the difference in arrival times at the two stations by comparing the recorded bit streams.

The signals recorded at all participating antennas are combined pairwise, thereby producing an interference pattern. The bit streams are shifted in time relative to each other until their cross-correlation function is maximized. It is necessary to have the approximate position of stations, sources and clock offsets to calculate an a priori time delay. The correlation process can then be limited to a “search window” of a few microseconds. The independent station clocks must remain synchronized well enough to obtain signal samples that will form a coherent interference pattern.

Most of the observing sessions are correlated with the Mark4/Mark5 correlators at the US Naval Observatory (Washington, USA), at the Max Planck Institute for Radio Astronomy (Bonn, Germany) and at Haystack Observatory (Westford, USA). Some sessions are correlated with the K4/K5 correlators in Kashima and Tsukuba, Japan, and some with the S2 correlator in Penticton, Canada. (Schlüter and Behrend, 2007)

3.7 Data – CONT05

CONT05 is a two-week campaign of continuous VLBI sessions, scheduled for observing during September 2005 and coordinated by the International VLBI Service for Geodesy and Astrometry (IVS). The observations started on September 12 at 17.00 UTC and ended on September 27.

The station network consisted of 11 stations:

| | | |
|------------------------------|----------------------------|-----------------------|
| Algonquin Park, Canada | Gilmore Creek, Alaska, USA | HartRAO, South Africa |
| Koike Park, Hawaii, USA | Ny Alesund, Norway | Onsala, Sweden |
| Svetloe, Russia | TIGO, Concepcion, Chile | Tsukuba, Japan |
| Westford, Massachusetts, USA | Wetzell, Germany | |

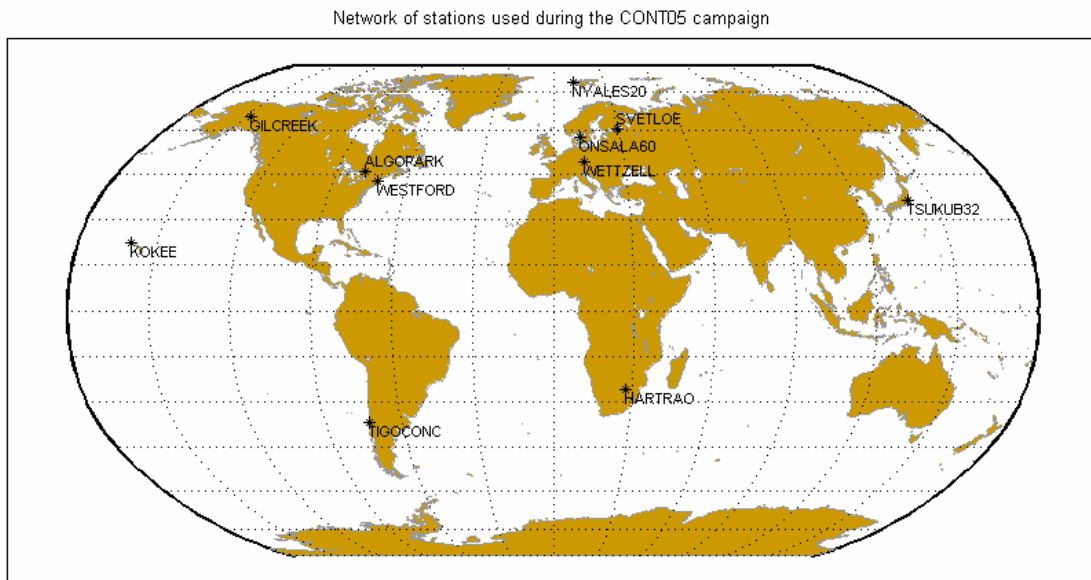


Figure (F 3.3): Station participating in the CONT05 campaign.

3.8 Software

At the Institute of Geodesy and Geophysics, TU Vienna, the OCCAM VLBI software package is used for VLBI data analysis. This software is transportable and freely distributed.

The roots of OCCAM go back to the eighties, when at the Geodetic Institute of the University of Bonn a software package for a VLBI data analysis called BVSS (Bonn VLBI Software System) was programmed. The goal in that time was to generate a software that is flexible to handle, easy to modify, and applicable more for special scientific investigations rather than for routine operations. The software included most of the geodynamical models to take into account all tidal influences on the rotation of the Earth, tidal deformation, various kinds of loading effects and also relativistic effects (Schuh, [1]).

The package consists of several executable programs, which must be used in strict order to compute the solution of a VLBI session. It is recommended to use powerful computers for data analysis because the modern observational experiments include a large number of observation. (Titov et al., 2004)

The input data format with OCCAM is the NGS-Format. NGS files can be downloaded from servers of the IVS.

OCCAM computes models and corrections to generate theoreticals for the observables, as well as partial derivatives for the adjustment. The adjustment can be carried out using three different methods: least squares method, least squares collocation method, and Kalman Filter.

Model computation menu

(Description based on OCCAM 6.0. User's guide (Titov et al., 2004))

1. Automatic model computation
2. Data handling
3. Precession and nutation
4. Station corrections and derivatives
5. Geometric model

1. Automatic model computation

This option is equivalent to manually running options 2, 3, 4, 5.

2. Data handling

This option reads the original VLBI data files for the experiment given in NGS-Format. From global Ephemeris and EOP catalogs the file EPHEM.DAT is created.

3. Precession and nutation

This program transforms between the J2000.0 Celestial Reference Frame for the quasars to their apparent positions at the observation time. EOP and Ephemeris data for Sun, Earth and Moon are read from EPHEM.DAT and interpolated to each observation epoch.

4. Station corrections and derivatives

- A. Corrections to the catalog station coordinates due to earth tides
- B. Furthermore, corrections such as antenna deformations, ocean loading, atmospheric loading, snow loading, soil moisture and non-tidal ocean loading and secular pole tide
- C. Antenna axis offset contribution to delays and rates
- D. Troposphere models
- E. Local source coordinates (azimuth, elevation, hour angle)
- F. Partial derivatives of the delay with respect to station, source coordinates, nutation parameters and ERP

The model for the solid earth tides used in OCCAM 6 is the model by Mathews and Dehant (1999), as recommended by the IERS Conventions 2003, except for the part of the permanent tide correction. In accordance with the conventional approach, the part for permanent tide has not been activated.

During my master thesis the main source-code was done within the subroutine “STATION $matthew.f$ ”, where the solid Earth tide model is stored.

5. Geometric model

This program computes the theoretical delay and rates for each observable included in the original data file. It considers the geometrical configuration of antennas and all relativistic effects.

4. Analysis and Simulations

4.1 Total tidal displacement

In this chapter the modelled time behaviour of surface deformations caused by solid Earth tides is presented in several plots. In Figures (F 4.2) and (F 4.3) the variation of displacement for one point on the Earth during one day (January 1st, 2006) is plotted in 30 minutes time steps in the geocentric (XYZ) and topocentric coordinate system (REN), respectively. To also see the displacement in the long-period tidal band, the time span was extended to one month (January 2006) for the same point. The resulting curves are plotted in Figure (F 4.4).

The deformation of the whole Earth is shown in Figures (F 4.5 – F 4.8) with a spatial resolution of $1^\circ \times 1^\circ$. For the vector's representation in (F 4.6) a $10^\circ \times 10^\circ$ grid was used. In all four figures the tidal displacement is modelled for January 1st, 2006 at 00 UTC. In addition, the time progression was computed for the whole day with two hours steps. These moving graphics are stored on the enclosed CD.

The computation was executed with the tidal model coded in the program *matthew.f*. The code of this program is an implementation of the solid Earth tide model, recommended in Chapter 7 of the IERS Conventions 2003 (McCarthy and Petit, 2004). For further details, see Chapter 4.3.

The input into this program is the time instant and location. The time information goes into the model as the Modified Julian Date (MJD). The station coordinates are needed in the geocentric system (XYZ). The output is the station displacement in geocentric coordinates (dx, dy, dz).

Geocentric coordinates of the perturbing bodies for the year 2006 are listed in file "EPHEM.06". The ephemerides for the bodies are given there with a temporal resolution of

12 hours. For the estimation of the position between these time instants, Lagrangian interpolation is carried out.

The current configuration of the perturbing bodies on January 1st, 2006 is shown in Figure (F 4.1), where the Sun's ephemerides are reduced by a factor of 100. The Moon and the Sun just passed through their closest position, when they were aligned at a new moon. So, January 1st is the first day after the day, when the amplitude of the tidal displacement reached the maximum and is now slowly decreasing. (The minimum will be in the first-quarter moon on January 6th.)

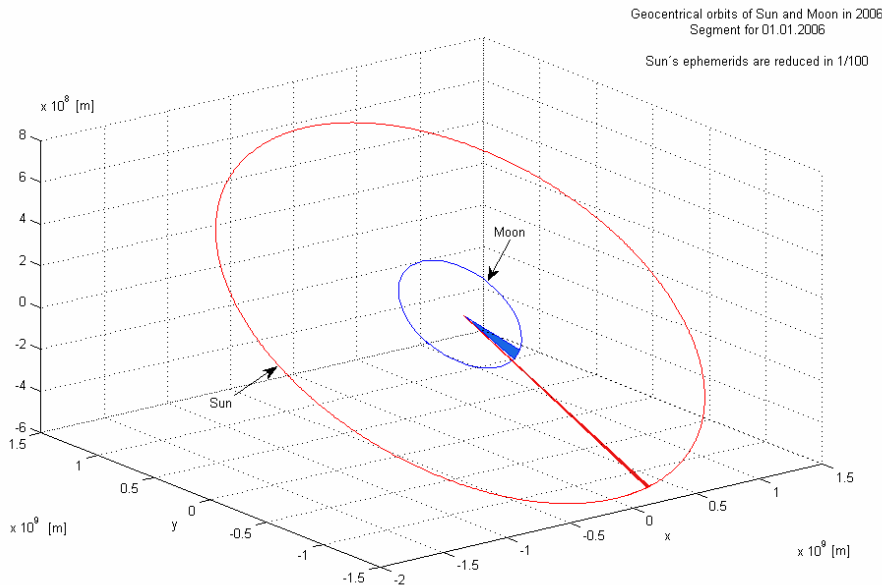


Figure (F 4.1): Geocentric orbits of the Sun and the Moon on January 1st, 2006. Sun's ephemerides are reduced by a factor of 100.

4.1.1 Tidal displacement at a station (15°E/50°N)

For the computation of the displacement due to the solid Earth tides, I chose a “virtual station” in Central Europe, placed at 15° East longitude and 50° North latitude.

The temporal variation of the geocentric coordinate differences (dX , dY , dZ) during the whole day is shown in Figure (F 4.2). The corresponding values are given in Table (T 4.1).

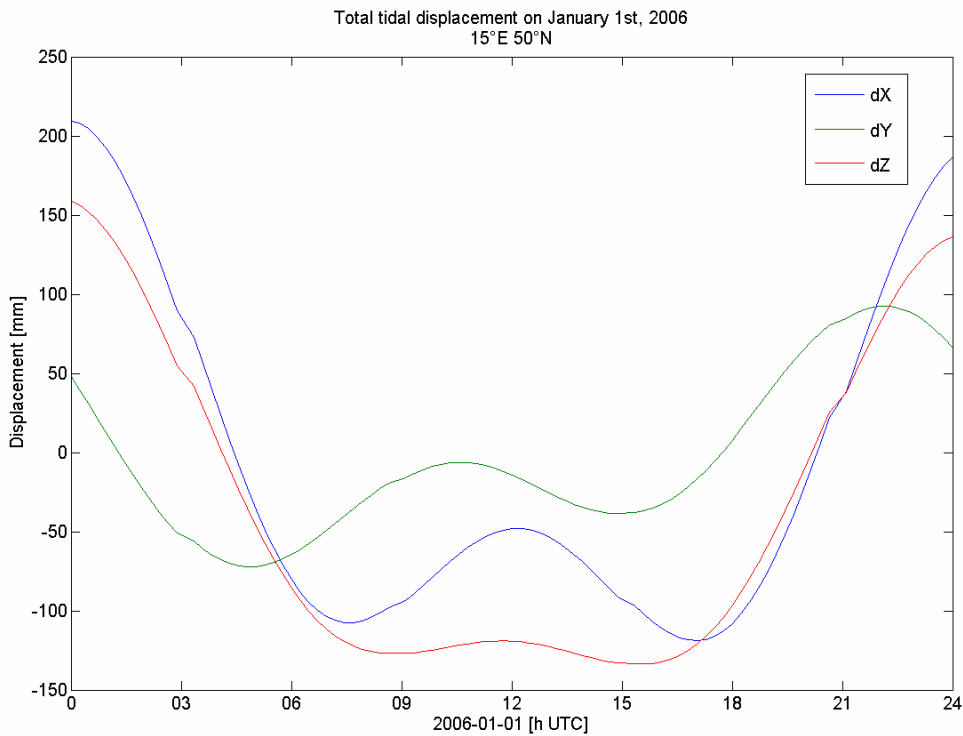


Figure (F 4.2): Tidal displacement in [mm] at 15°E/50°N in geocentric XYZ coordinates on January 1st, 2006.

| MJD | dX [mm] | dY [mm] | dZ [mm] | | MJD | dX [mm] | dY [mm] | dZ [mm] |
|----------|---------|---------|---------|--|----------|---------|---------|---------|
| 53736.00 | 210.3 | 48.3 | 159.5 | | 53736.50 | -47.7 | -13.7 | -118.7 |
| 53736.04 | 193.5 | 12.8 | 141.0 | | 53736.54 | -52.3 | -24.5 | -121.8 |
| 53736.08 | 150.7 | -22.3 | 104.3 | | 53736.58 | -68.7 | -34.3 | -127.7 |
| 53736.12 | 90.3 | -50.6 | 55.7 | | 53736.62 | -91.2 | -38.3 | -132.8 |
| 53736.17 | 24.1 | -67.8 | 3.0 | | 53736.67 | -111.1 | -32.8 | -132.0 |
| 53736.21 | -36.0 | -72.0 | -45.9 | | 53736.71 | -119.3 | -16.9 | -121.0 |
| 53736.25 | -80.4 | -64.5 | -85.0 | | 53736.75 | -108.7 | 7.6 | -97.0 |
| 53736.29 | -103.9 | -49.1 | -111.0 | | 53736.79 | -76.6 | 36.6 | -59.9 |
| 53736.33 | -106.8 | -31.0 | -124.0 | | 53736.83 | -25.2 | 64.1 | -13.1 |
| 53736.38 | -94.1 | -15.7 | -126.6 | | 53736.88 | 37.9 | 84.2 | 37.3 |
| 53736.42 | -74.1 | -7.0 | -123.6 | | 53736.92 | 102.0 | 92.2 | 83.9 |
| 53736.46 | -56.2 | -6.7 | -119.8 | | 53736.96 | 155.2 | 85.8 | 119.0 |
| | | | | | 53737.00 | 187.4 | 65.9 | 136.8 |

Table (T 4.1): Corresponds to (F 4.2). Presented values for tidal displacement at 15°E/50°N are with one-hour resolution.

In the topocentric coordinates (F 4.3) the displacement is separated into radial and tangential components. In radial direction, the displacement is approximately ten times larger, than in the transverse directions. The height difference between the maximum amplitude at 00 UTC and the minimum amplitude at 16 UTC is 43.8 cm. From the Figure, it can be seen that the displacement shows two local maxima and two local minima during the whole day. It starts at

00 UTC on the “opposite bulge”, with respect to the Moon and the Sun, then it arrives due to the Earth’s rotation in the area, where the depression of the surface takes place (approx. 4 UTC – 20 UTC). During this time interval, it achieves a local maximum at about 12 UTC, where its distance to the bulge under the perturbing bodies is the shortest. After 20 UTC, the surface is lifted again.

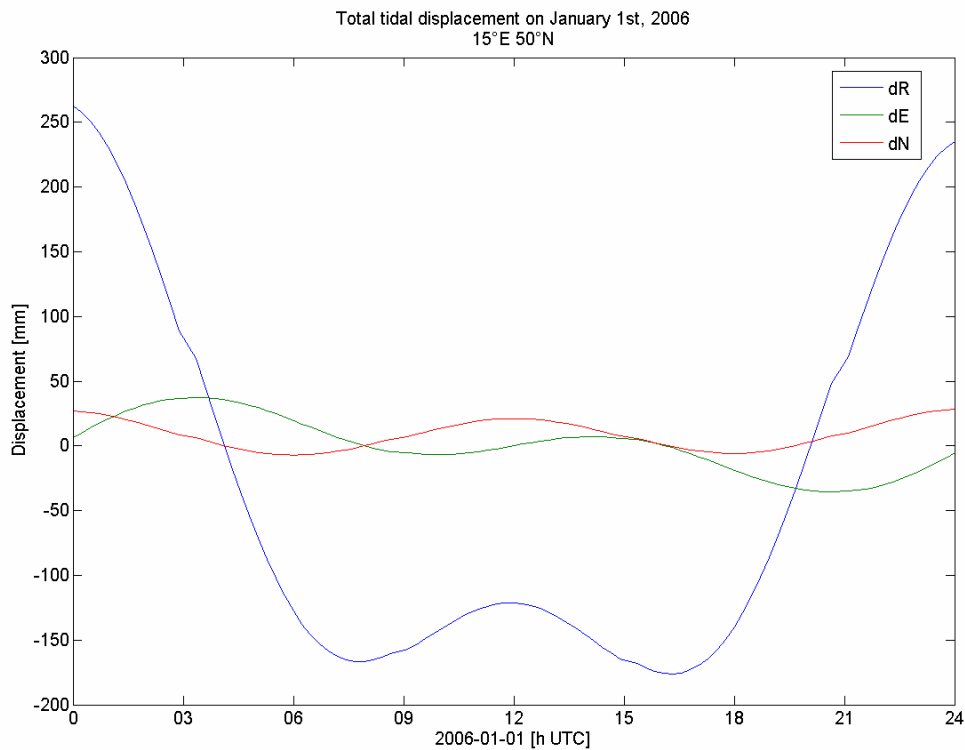


Figure (F 4.3): Tidal displacement at 15°E/50°N in topocentric REN coordinates on January 1st, 2006.

| MJD | dR [mm] | dE [mm] | dN [mm] | | MJD | dR [mm] | dE [mm] | dN [mm] |
|-----------------|---------|---------|---------|--|-----------------|---------|---------|---------|
| 53736.00 | 262.7 | 5.9 | 27.0 | | 53736.50 | -121.3 | 0.1 | 21.1 |
| 53736.04 | 231.1 | 20.6 | 23.5 | | 53736.54 | -128.7 | 4.6 | 19.4 |
| 53736.08 | 169.4 | 31.5 | 16.8 | | 53736.58 | -145.6 | 7.0 | 14.4 |
| 53736.12 | 89.1 | 36.7 | 8.4 | | 53736.62 | -164.5 | 5.8 | 7.6 |
| 53736.17 | 4.2 | 35.7 | 0.5 | | 53736.67 | -175.7 | 0.4 | 0.8 |
| 53736.21 | -71.5 | 29.4 | -5.1 | | 53736.71 | -169.6 | -8.4 | -4.2 |
| 53736.25 | -127.4 | 19.7 | -7.1 | | 53736.75 | -140.0 | -18.7 | -5.8 |
| 53736.29 | -158.7 | 9.1 | -5.2 | | 53736.79 | -86.1 | -28.2 | -3.7 |
| 53736.33 | -166.5 | 0.1 | 0.0 | | 53736.83 | -13.0 | -34.2 | 2.0 |
| 53736.38 | -157.2 | -5.5 | 7.0 | | 53736.88 | 68.9 | -35.1 | 9.9 |
| 53736.42 | -140.5 | -6.8 | 14.1 | | 53736.92 | 146.1 | -30.1 | 18.1 |
| 53736.46 | -126.1 | -4.5 | 19.2 | | 53736.96 | 205.0 | -19.6 | 24.7 |
| | | | | | 53737.00 | 234.8 | -5.6 | 28.3 |

Table (T 4.2): Corresponds to (F 4.3). Presented values for tidal displacement at 15°E/50°N are with one-hour resolution.

Tidal movement during a month

In Figure (F 4.4) the movement of the same point (15°E/50°N) is plotted for a period of a month. The largest amplitudes can be seen around the new moon (December 31st) and full moon (January 14th) when Sun, Moon and Earth form a line and the tidal forces due to the Sun reinforce those of the Moon. It can be seen, that the amplitude at the full moon is actually a little bit smaller, than the one at the new moon.

When the Moon is at first quarter (January 6th) or third quarter (January 21st), Sun and Moon are separated by 90° and the forces due to the Sun partially cancel those of the Moon. At these points in the lunar cycle, the tide reaches its minimum.

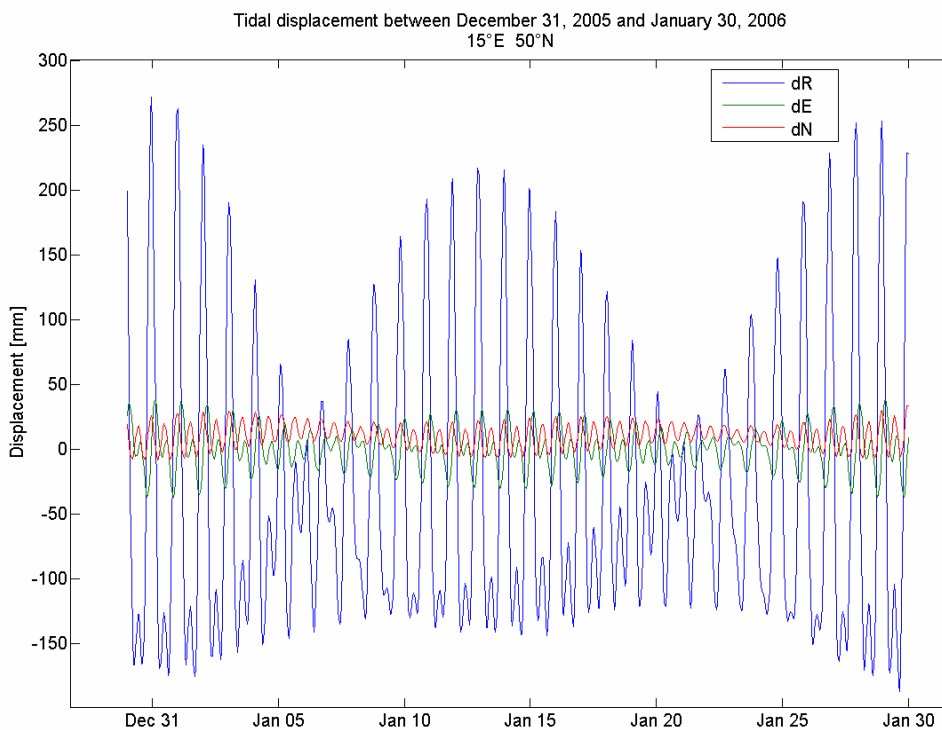


Figure (F 4.4): Tidal displacement at 15°E/50°N during a month (December 31st, 2005 and January 1st, 2006) in topocentric REN coordinates.

4.1.2 Global tidal displacement

In Figure (F 4.5) the tidal deformation for the whole Earth on 1st January 2006 at 00 UTC in radial direction is plotted. The displacement transverse to radial direction is shown in Figure

(F 4.6), where the East and North components are put together. In the Figures (F 4.7) and (F 4.8) the transverse components are displayed separately. Corresponding values of the displacement are stored in txt-files on the enclosed CD.

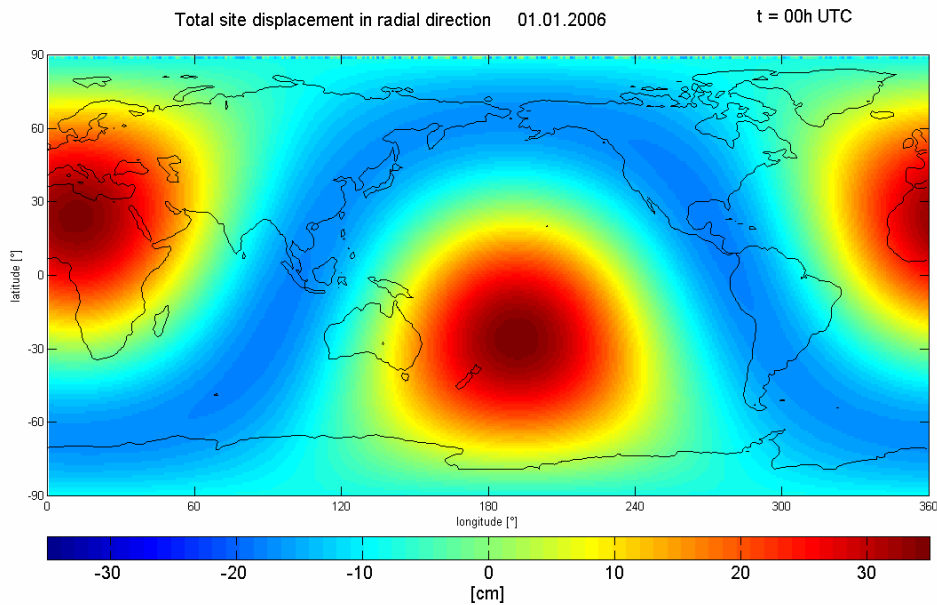


Figure (F 4.5): Radial component of total tidal displacement on January 1st, 2006 at 00h UTC.

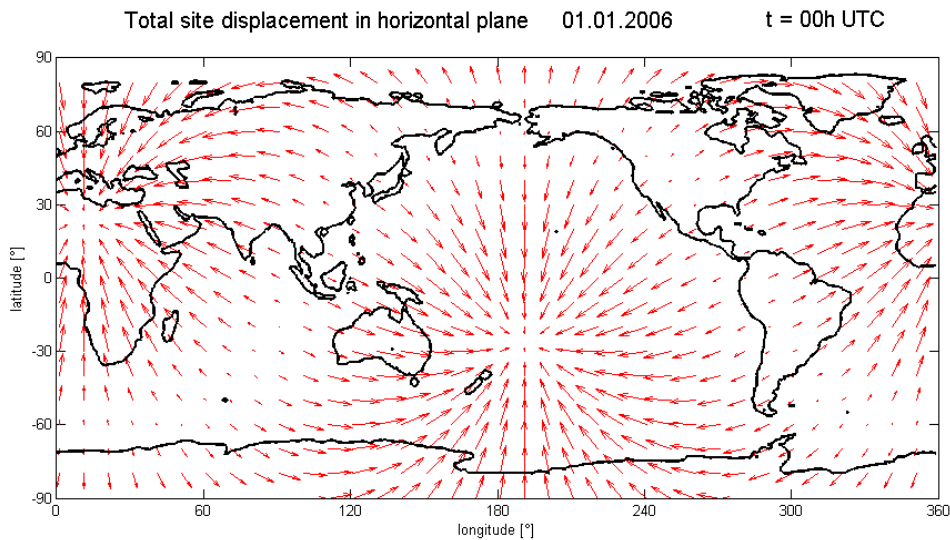


Figure (F 4.6): Site displacement in the transverse directions on January 1st, 2006 at 00h UTC.

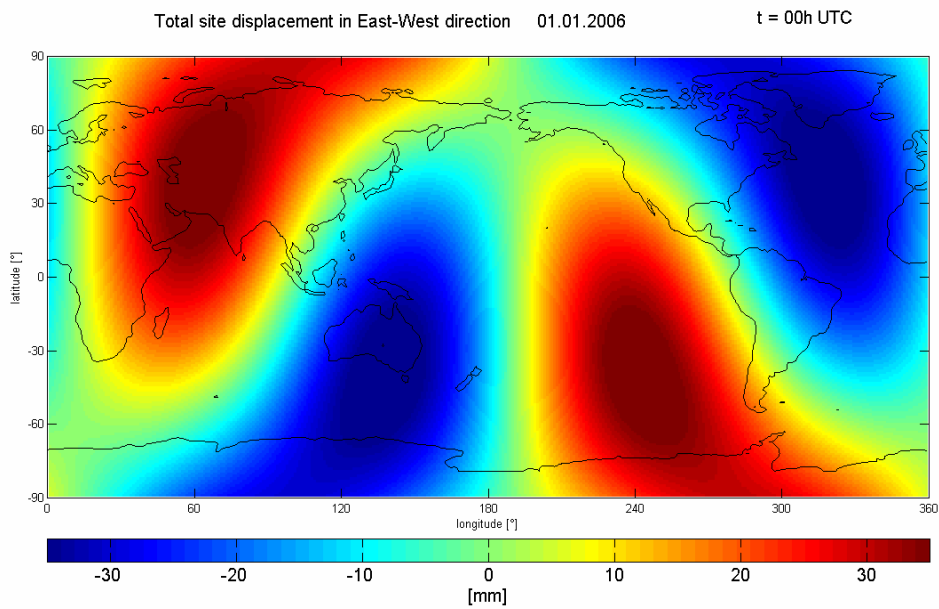


Figure (F 4.7): East component of total tidal displacement on January 1st, 2006 at 00h UTC.

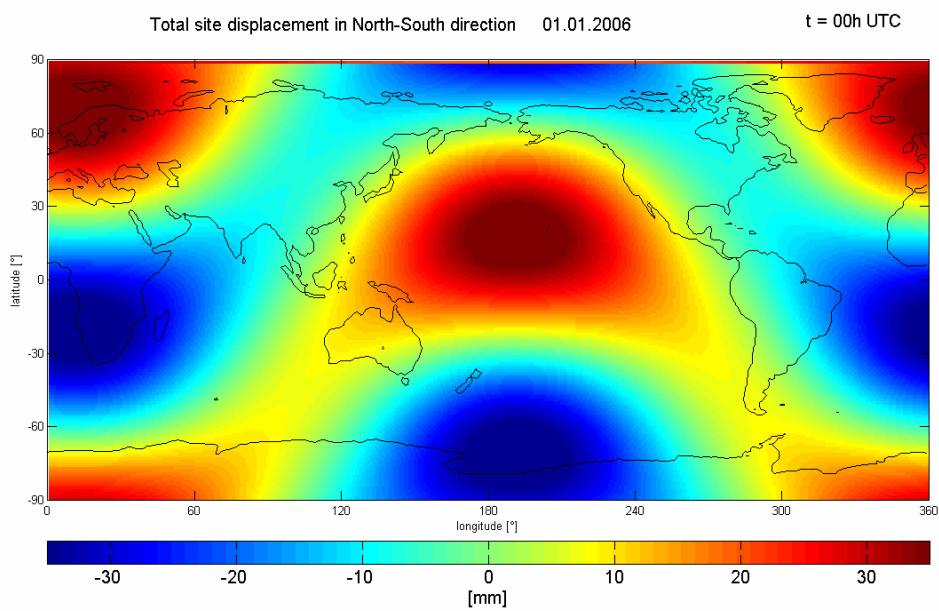


Figure (F 4.8): North component of total tidal displacement on January 1st, 2006 at 00h UTC.

4.2 Radial components of tidal displacement following the IERS Conventions 2003

In the following Figures (F 4.9 – F 4.17) the individual components with their contribution to the total tidal displacement in radial direction are visualised. The snap shots are taken again for January 1st 2006 at 00 UTC.

Figure (F 4.9) shows the contribution to the displacement from the latitude dependence in the nominal Love number $h_2 = 0.6078$. The contribution to the Love number was discussed in Chapter 1.4.1 Table (T 1.7).

In Figures (F 4.10) and (F 4.11) the displacement arising from second degree tidal potential is divided into the contributions of the Moon and the Sun, respectively.

The same separation is shown in (F 4.12) and (F 4.13), where the forcing potential is of third degree. In Figure (F 4.13) it can be seen, that the contribution of the Sun is quite ignorable. The largest displacement is only 0.01 mm.

Table (T 4.3) gives an overview about the practical process of the correction's computation. The theoretical approach is described in Chapter 1.4. Numbers in the second column are the equations presented in the IERS Conventions 2003 (McCarthy and Petit, 2004). In the third column, the corresponding subroutines from the “*matthew.f*” file are listed and last column shows the numbers of the matching figures.

| Corrections for | IERS Conventions 2003 | subroutines in <i>matthew.f</i> | Figure |
|--|-----------------------|---------------------------------|----------|
| Step 1 | | | |
| the out of phase contributions from $h_{21}^{(0)l}$ and $l_{21}^{(0)l}$ | 14a, 14b | ST1IDIU | (F 4.14) |
| the out of phase contributions from $h_{22}^{(0)l}$ and $l_{22}^{(0)l}$ | 15a, 15b | ST1ISEM | (F 4.15) |
| the latitude dependence in transverse displacement due to $l^{(1)}$ term | 12, 13 | ST1L1 | --- |

| Step 2 | | | |
|--|-----------------|----------|----------|
| frequency dependence in the diurnal band | <i>16a, 16b</i> | STEP2DIU | (F 4.16) |
| frequency dependence in the long period band | <i>17a, 17b</i> | STEP2LON | (F 4.17) |

Table (T 4.3): Corrections for station coordinates variation due to solid Earth tides. The equivalence between IERS Conventions 2003 and OCCAM source-code is shown.

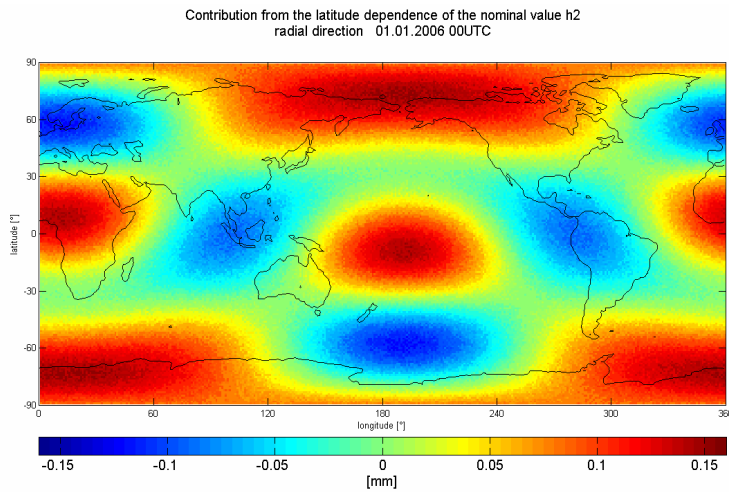


Figure (F 4.9): Contribution to displacement in radial direction of the latitude dependence of the nominal value h_2 on January 1st, 2006 at 00h UTC.

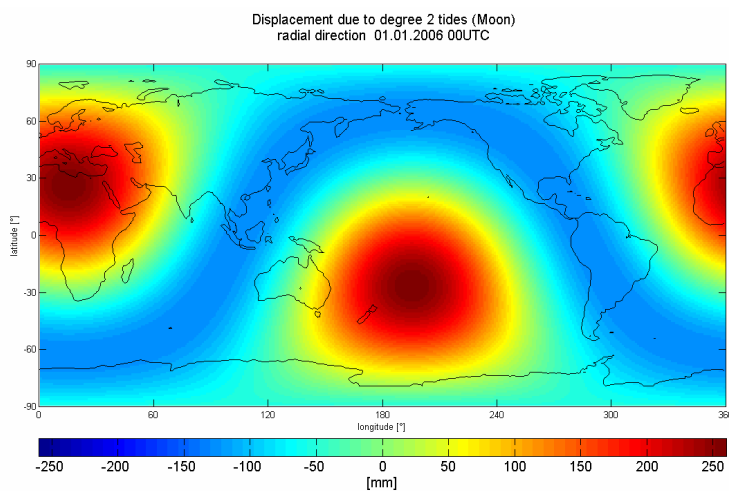


Figure (F 4.10): Displacements in radial direction due to second degree tides on January 1st, 2006 at 00h UTC, only Moon's contribution.

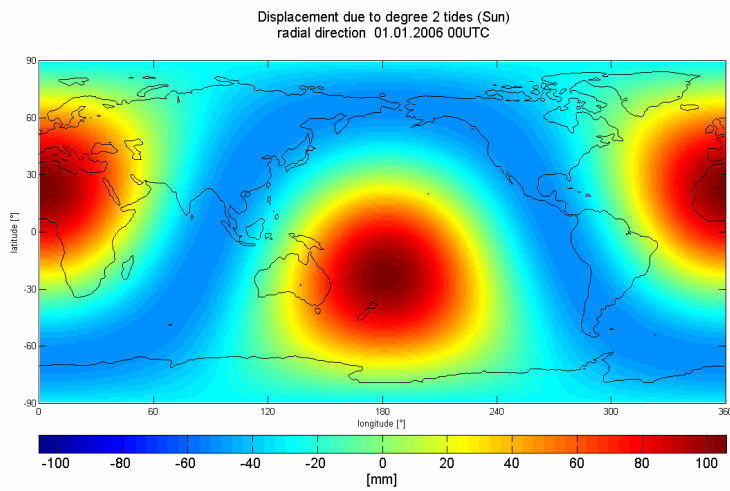


Figure (F 4.11): Displacements in radial direction due to second degree tides on January 1st, 2006 at 00h UTC, only Sun's contribution.

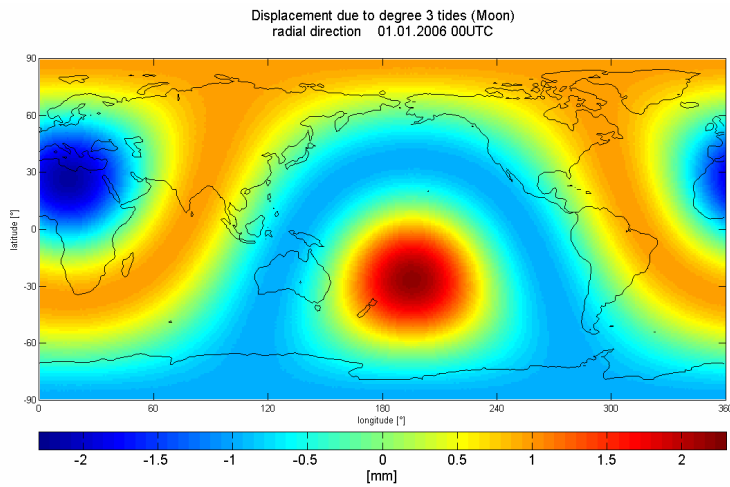


Figure (F 4.12): Displacements in radial direction due to third degree tides on January 1st, 2006 at 00h UTC, only Moon's contribution.

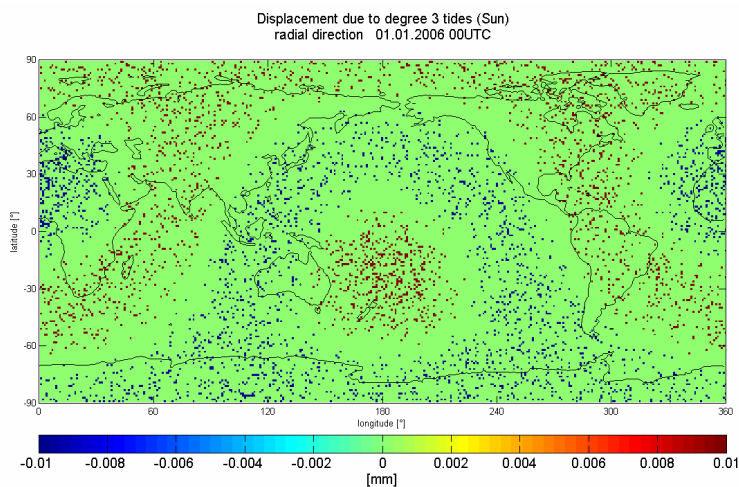


Figure (F 4.13): Displacements in radial direction due to third degree tides on January 1st, 2006 at 00h UTC, only Sun's contribution – ignorable.

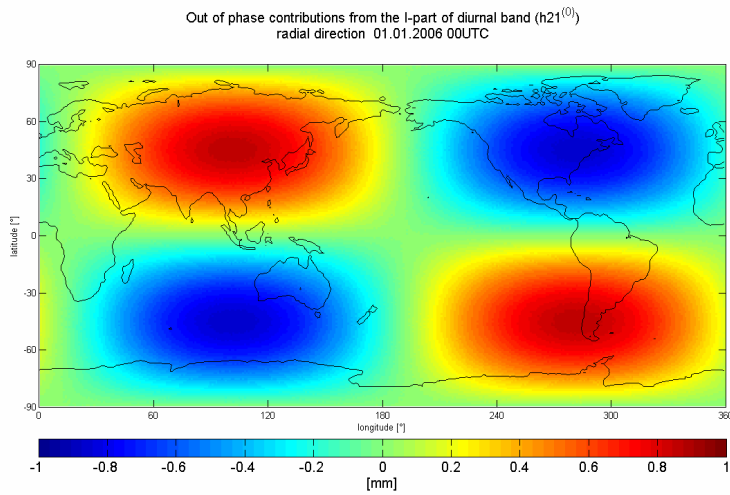


Figure (F 4.14): Corrections to displacement in radial direction for the out of phase part of diurnal band ($h_{21}^{(0)I}$) on January 1st, 2006 at 00h UTC.

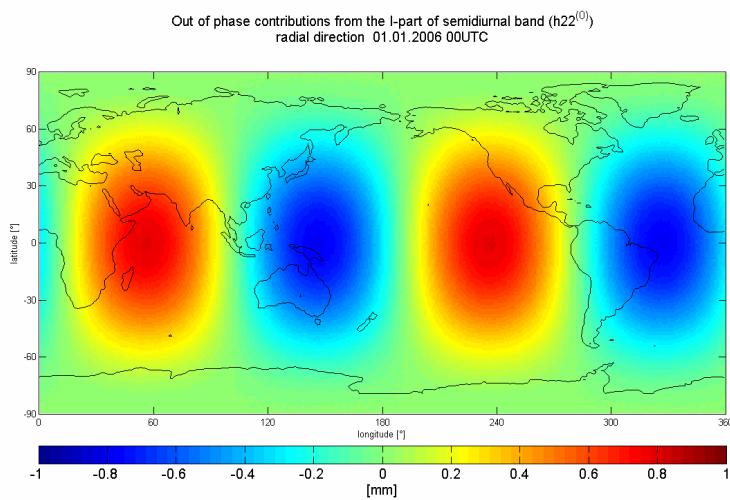


Figure (F 4.15): Corrections to displacement in radial direction for the out of phase part of semidiurnal band ($h_{22}^{(0)I}$) on January 1st, 2006 at 00h UTC.

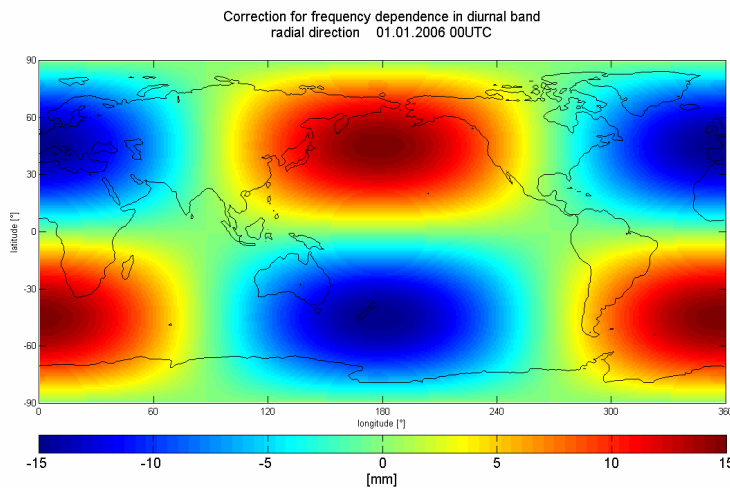


Figure (F 4.16): Corrections to displacement in radial direction for frequency dependence in diurnal band (in phase and out of phase) on January 1st, 2006 at 00h UTC.

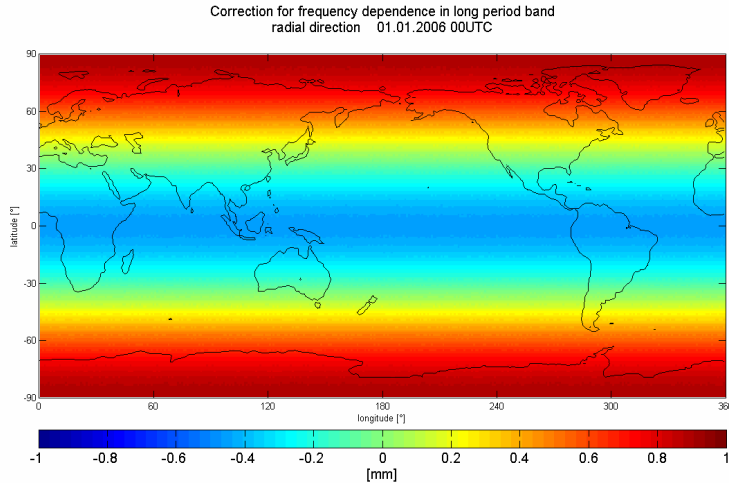


Figure (F 4.17): Corrections to displacement in radial direction for frequency dependence in long period band (in phase and out of phase) on January 1st, 2006 at 00h UTC.

4.3 Matlab simulation

the program “*LN_FCN.m*” was written in the software Matlab to determinate the Love numbers from the tidal displacements. The algorithm was then used in OCCAM software to analyze the real data.

Because the input parameters to the simulation program are known, they can be compared with the adjusted values in the output and the user is immediately warned about bugs.

Coordinates of all 11 stations, which participated in the CONT05 campaign, and 19 radio source positions (selected from the ICRF catalogue) are input to the program. Coordinates of the Moon and the Sun are adopted from the “EPHEM.06” file.

The output parameters from the least-squares adjustment are the nominal Love number h_2 , the nominal Shida number l_2 , and 6 frequency dependent Love numbers from the diurnal band ($h_{2l}(O_1)$, $h_{2l}(P_1)$, $h_{2l}(K_1)$, $h_{2l}(\psi_1)$, $h_{2l}(\Phi_1)$, $h_{2l}(J_1)$). The program continues with these six diurnal Love numbers to estimate the frequency of the Nearly Diurnal Free Wobble (associated with the Free Core Nutation) and the resonance strength factor h_{RS} . Because there is no linear dependence with respect to the NDFW period in the resonance formula (E 2.1), the solution of the equation is obtained with a sufficient number of iterations.

4.3.1 Input data

Stations

| Station | X [m] | Y [m] | Z [m] |
|----------|--------------|--------------|--------------|
| GILCREEK | -2281547.303 | -1453645.078 | 5756993.149 |
| KOKEE | -5543837.621 | -2054567.852 | 2387851.922 |
| SVETLOE | 2730173.860 | 1562442.670 | 5529969.070 |
| WETZELL | 4075539.895 | 931735.270 | 4801629.355 |
| WESTFORD | 1492206.597 | -4458130.517 | 4296015.532 |
| NYALES20 | 1202462.761 | 252734.404 | 6237766.013 |
| ONSLA60 | 3370606.043 | 711917.494 | 5349830.735 |
| TSUKUB32 | -3957408.308 | 3310229.259 | 3737494.482 |
| HARTRAO | 5085442.796 | 2668263.498 | -2768697.043 |
| TIGOCONC | 1492054.257 | -4887960.956 | -3803541.320 |
| ALGOPARK | 918034.750 | -4346132.269 | 4561971.156 |

Table (T 4.4): Real station coordinates were used in the simulation program.

The program uses the stations, which participated in the CONT05 campaign. These are defined with geocentric coordinates (X, Y, Z), which were taken from the ITRF97 catalogue.

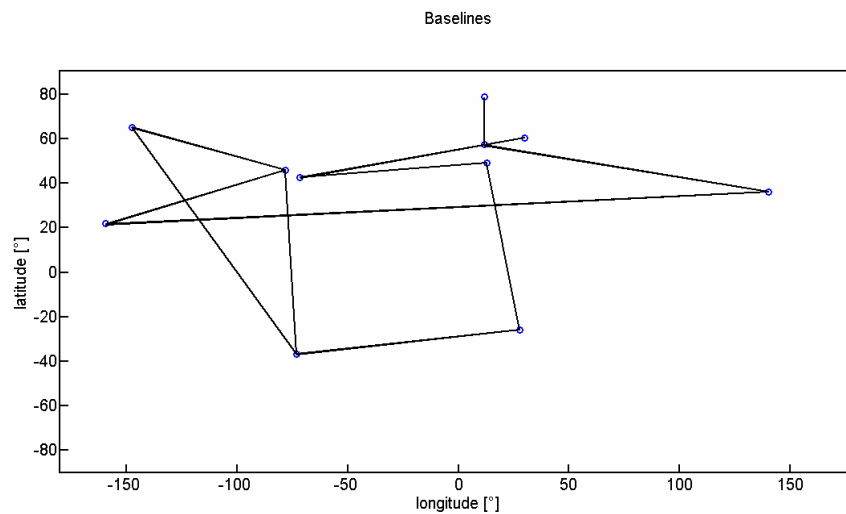


Figure (F 4.18): For the simulations, 11 baselines were selected.

Celestial Reference Frame

For the realisation of the celestial reference frame, 19 radio sources from the ICRF catalogue were selected. Their equatorial coordinates (Right Ascension and Declination) are given w.r.t. J2000.0.

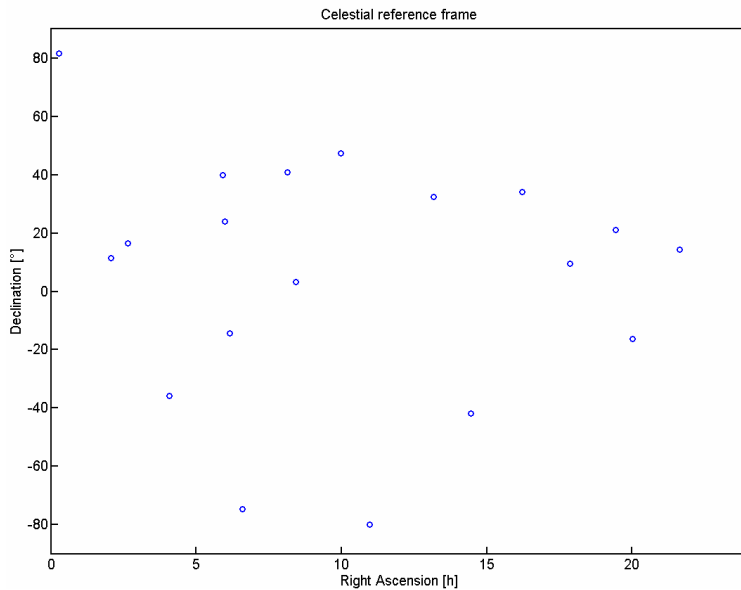


Figure (F 4.19): 19 ICRF radio sources used for the simulation program.

Position of the attracting bodies

The coordinates from the Moon and the Sun are given in geocentric inertial system.

| MJD | X [m] | Y [m] | Z [m] | |
|-------------|-------------------|----------------------|---------------------|-------|
| 53729.00000 | 8233593836.163701 | -134784046257.976196 | -58433977955.871803 | %Sun |
| 53729.00000 | -379756749.395463 | -100612704.007153 | -48096337.887375 | %Moon |
| 53729.02083 | 8288000159.227712 | -134781118557.961761 | -58432710734.116676 | %Sun |
| 53729.02083 | -379161074.083406 | -102083087.396467 | -48901730.317899 | %Moon |
| 53729.04167 | 8342431580.075037 | -134778171223.183777 | -58431434999.754890 | %Sun |
| 53729.04167 | -378556971.727286 | -103552039.731435 | -49706485.346676 | %Moon |
| ... | ... | ... | ... | |

Table (T 4.5): Geocentric positions of the perturbing bodies. The program starts with ephemerides from January 1st, 2006.

Positions from 01.01.2006 to 10.01.2006 (MJD: 53729 – 53739) in 30 min steps are used in the simulation program. The values at the epochs of the observations were estimated with Lagrangian interpolation from the coordinates given in “EPHEM.06”, with a temporal resolution of 12 hours.

4.3.2 Computation procedure

The computation runs in a loop over the epochs. As mentioned above, I chose 10 days for the computation. Because the time step between the observations is 30 minutes, the program uses 480 simulated observation epochs. The number of observations differs in each epoch, because the current geometry between baselines and sources needs to be taken into account. The

maximal amount of observations is 67, whereas the minimum is 27. From each loop the partial derivatives of the tidal displacements for 8 parameters, i.e., h_2 , l_2 , $h_{2I}(O_1)$, $h_{2I}(P_1)$, $h_{2I}(K_1)$, $h_{2I}(\Psi_1)$, $h_{2I}(\Phi_1)$, $h_{2I}(J_1)$ are obtained. These parameters are adjusted with the least-squares method (LSM). The LSM is used to adjust the parameters of the model to get an optimal fit of the data obtained from observations. The “optimal fit” means that the sum of squared residuals (difference between an observed value and the value given by the model) is a minimum. The final A-matrix (design matrix with partial derivatives) has 8 columns (8 parameters) and the number of rows corresponds to the total number of observations, i.e., 20830. (see T 4.8).

Next step is the determination of ω_{FCN} . The defining Equation (E 2.1) is not linear with respect to this parameter and the estimation needs to be done through an iterative process. In the LSM adjustment, ω_{FCN} is estimated together with h_{RS} and $h_{2I}(O_1)$. As an input, i.e. as observations, the six estimated frequency dependent Love numbers are used.

Detailed description of the program “LN_FCN.m”

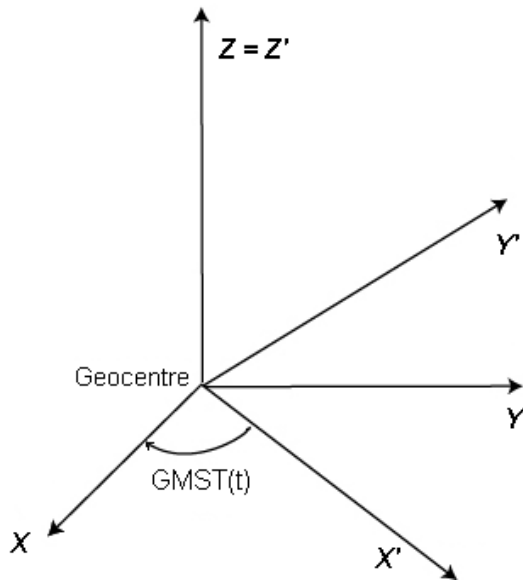


Figure (F 4.20): Geocentric coordinate systems: Earth-fixed and quasi-inertial.

For the computation, a geocentric coordinate system was chosen, which rotates with the Earth’s body. The origin of this system is situated at the Earth’s centre of mass, the X-axis points through the intersection of equator and Greenwich meridian, the Y-axis is positive to the east and the Z-axis goes through the pole of the ITRF.

The coordinates of the Moon, the Sun and radio sources are given in a geocentric coordinate system, which is inertial (inertial in the sense that it does not co-rotate with the Earth). The X'-axis points to the vernal equinox, the Z'-axis is identical with the Z-axis of the Earth’s fix system, and the Y'-axis completes the system to a right-hand system.

The rotation is related to the angle GMST. Greenwich Mean Sidereal Time (GMST) is the hour angle between the Greenwich meridian and the vernal equinox measured westward along the celestial equator.

The next step requires the computation of the displacement for each station in the local system (REN) with Equation (E 1.32) for the radial direction and Equations (E 1.30 – E 1.31) for directions to east and north, respectively. The nominal values of Love numbers are $h_2 = 0.6078$ and $l_2 = 0.0847$. To this nominal displacement due to the second degree tidal potential, corrections for radial displacement (E 4.1) are added through 6 frequency dependent diurnal constituents. Their descriptions are listed in Tables (T 1.3) and (T 4.6).

$$\delta u_{r(f)} = -\frac{3}{2} \sqrt{\frac{5}{24\pi}} H_f \delta h_{21}(f) \sin(2\Phi) \sin(\theta_f + \lambda) \quad (\text{E 4.1})$$

H_f Cartwright-Tayler amplitude of the tidal term
 $\delta h_{21}(f)$ difference of $h_{21}(f)$ from the nominal value h_2
 (Φ, λ) station coordinates
 θ_f tidal argument

| Tide | Love number $h_{21}(f)$ (IERS2003) | Cartwright-Tayler amplitude H_f [mm] (Values in (T 1.3) converted with factor f_{21}) | Argument (θ_f) (from T 1.3) |
|----------------|---------------------------------------|---|---|
| O ₁ | 0.6028 | -262 | $\tau - s$ |
| P ₁ | 0.5817 | -122 | $t - h$ |
| K ₁ | 0.5236 | 369 | $\tau + s$ |
| ψ_1 | 1.0569 | 3 | $(t + h) + (h - p_s)$ |
| Φ_1 | 0.6645 | 5 | $t + 3h$ |
| J ₁ | 0.6108 | 21 | $(\tau + s) + (s - p)$ |

Table (T 4.6): Input parameters for the 6 diurnal waves: frequency dependent Love number $h_{21}(f)$, amplitude H_f in millimetres and tidal argument (θ_f).

| Doodson's fundamental arguments (see also Ch 1.2.2) |
|---|
| $\tau = \text{GMST} - s'$ $\text{GMST} = \text{fhr} \cdot 15 + 280.4606184 + 36000.7700536 \cdot T + 0.00038793 \cdot T^2 - 0.0000000258 \cdot T^3$ $s' = 218.31664563 + 481267.88194 \cdot T - 0.0014663889 \cdot T^2 + 0.00000185139 \cdot T^3$ |
| $s = s' + \text{Pr}$ $\text{Pr} = 1.396971278 \cdot T + 0.000308889 \cdot T^2 + 0.000000021 \cdot T^3 + 0.000000007 \cdot T^4$ |
| $h = 280.46645 + 36000.7697489 \cdot T + 0.00030322222 \cdot T^2 + 0.00000002 \cdot T^3 - 0.00000000654 \cdot T^4$ |
| $p = 83.35324312 + 4069.01363525 \cdot T - 0.01032172222 \cdot T^2 - 0.0000124991 \cdot T^3 + 0.00000005263 \cdot T^4$ |
| $N' = 234.95544499 + 1934.13626197 \cdot T - 0.00207561111 \cdot T^2 - 0.00000213944 \cdot T^3 + 0.0000000165 \cdot T^4$ |
| $p_s = 282.93734098 + 1.71945766667 \cdot T + 0.00045688889 \cdot T^2 - 0.00000001778 \cdot T^3 - 0.00000000334 \cdot T^4$ |
| T: time expressed in Julian centuries, starting with 2000 January 01, at 12 UT |

Table (T 4.7): Doodson's fundamental arguments.

The equation for the real part of radial displacement due to the tidal term of frequency f (E 4.1) is obtained from the defining equation (E 4.2) given in [“(16a)” IERS2003 p.81].

$$\delta u_{r(f)} = \left[\delta R_f \sin(\theta_f + \lambda) \right] \sin(2\Phi) \quad (\text{E 4.2})$$

where

$$\delta R_f = -\frac{3}{2} \sqrt{\frac{5}{24\pi}} H_f \delta h_f \quad \delta h_f = h_{21}(f) - h_2$$

The total displacement is transformed from the local system to the geocentric Earth-fixed system by rotations around $Z(\lambda)$ and $Y(\Phi)$ axis. Hereby, the coordinate shifts due to the modelled tidal displacement are expressed in X, Y, and Z direction.

Then, for each baseline two baseline vectors (F 4.19) are computed. The “observed” one comes from coordinate differences of the stations, which are changed by the tides. The “computed” baseline vector is the reference without tides, i.e., simply the difference between the ITRF station coordinates.

Observations, in units of metres, are defined as the time difference between arrival times of the wavefront at the baseline stations multiplied by speed of light. In the simulation, observations are obtained by multiplication of the baseline vector with the unit vector in source direction. The observations are computed for the “observed” and for the “computed”

baseline vectors. The difference between these two values goes into the L-vector in the least-squares adjustment, see Equation (E 4.9).

The A-matrix in the adjustment is filled with partial derivatives of the tidal displacement with respect to the estimated Love numbers (Table T 4.8).

Because the L-vector contains the differences of the observations in the source direction, it is essential to have the partial derivatives in the A-matrix also in this particular direction. Thus, the values need to be transformed from the local coordinate system (REN) with the zenith angle ($z_{stl(2)}$) and azimuth ($az_{stl(2)}$) into source direction, where $stl(2)$ in the argument stands for one of the baseline stations.

The tidal displacement function u , used in Equations (E 4.3 – E 4.5) is defined in (E 1.30 – E 1.31). For the frequency dependent correction of the displacement $\delta u_{r(f)}$ see Equation (E 4.1).

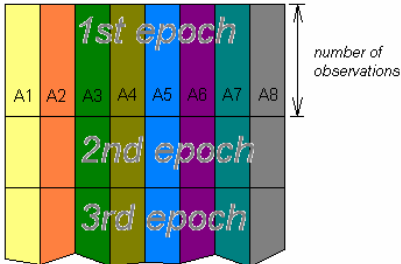
| | | |
|---|------------------------------------|---|
|  <p style="text-align: center;">A - matrix</p> | A1 h_2 | $\frac{\partial u_{r,st1}}{\partial h_2} \cdot \cos(z_{st1}) - \frac{\partial u_{r,st2}}{\partial h_2} \cdot \cos(z_{st2})$ <p style="text-align: right;">(E 4.3)</p> |
| | A2 l_2 | $\left(\frac{\partial u_{\lambda,st1}}{\partial l_2} \cdot \sin(az_{st1}) + \frac{\partial u_{\lambda,st1}}{\partial l_2} \cdot \cos(az_{st1}) \right) -$ $- \left(\frac{\partial u_{\lambda,st2}}{\partial l_2} \cdot \sin(az_{st2}) + \frac{\partial u_{\lambda,st2}}{\partial l_2} \cdot \cos(az_{st2}) \right)$ <p style="text-align: right;">(E 4.4)</p> |
| | A3-A8 $\delta h_{2l}(f)$ | $\frac{\partial \delta u_{r(f),st1}}{\partial \delta h_{2l}(f)} \cdot \cos(z_{st1}) - \frac{\partial \delta u_{r(f),st2}}{\partial \delta h_{2l}(f)} \cdot \cos(z_{st2})$ <p style="text-align: right;">(E 4.5)</p> |

Table (T 4.8): Structure of the design matrix A (20830, 8) filled with partial derivatives of the tidal displacement function.

A test, added in the program, discovers simulated observations with a zenith distance larger than 90°. If this case happens, a warning message is displayed:

!!! ERROR !!!

Zenit distance at these stations to sources is more than 90deg!

Do not use this combination!

and the program is terminated.

In addition, it is stated for which time epoch the observation has been excluded.

The resonance formula for the Love numbers of specific tide in the diurnal band $h_{21}(f)$ (E 2.1) contains the FCN frequency in the terrestrial reference frame in which we are interested. Equation (E 2.1) is solved for $h_{21}(O_1)$, h_{RS} and ω_{FCN} . Because of the non-linear dependence of ω_{FCN} , iterations need to be carried out for ω_{FCN} and h_{RS} .

In the LSM adjustment the L-vector is filled with the six frequency dependent Love numbers of the previous part of the program.

The A-matrix is filled with partials derivatives of Equation (E 2.1) with respect to $h_{21}(O_1)$, h_{RS} and ω_{FCN} (E 4.6 – E 4.8).

$$\frac{\partial h_{21}(f)}{\partial h_{21}(O_1)} = 1 \quad (E 4.6)$$

$$\frac{\partial h_{21}(f)}{\partial h_{RS}} = \frac{\omega_f - \omega_{O_1}}{\omega_{FCN} - \omega_f} \quad (E 4.7)$$

$$\frac{\partial h_{21}(f)}{\partial \omega_{FCN}} = h_{RS} \cdot \left(- \frac{\omega_f - \omega_{O_1}}{(\omega_{FCN} - \omega_f)^2} \right) \quad (E 4.8)$$

where the Equations (E 4.7) and (E 4.8) are equal to zero for the reference tidal wave O_1 .

4.3.3 Output values

The adjusted mean values in the vector X are obtained with the least-squares method (E 4.9). Corresponding formal errors σ_x , (i.e. a measure how tightly all the computed values are clustered around the mean) are defined in Equation (E 4.10)

$$X = (A^T \cdot A)^{-1} \cdot A^T \cdot L \quad (E 4.9)$$

$$\sigma_x = \sqrt{\text{var}(X)} \quad \text{var}(X) = \text{diag}(A^T \cdot A)^{-1} \quad (E 4.10)$$

The obtained adjusted values from the simulation program for h_2 , l_2 , $h_{2l}(O_1)$, $h_{2l}(P_1)$, $h_{2l}(K_1)$, $h_{2l}(\psi_1)$, $h_{2l}(\Phi_1)$, $h_{2l}(J_1)$ are identical with the input values. This confirms that there are no mistakes in the source code when evaluating the partial derivatives of the tidal displacement. However, one can see that the formal errors for the Love number corresponding to the ψ_1 tide and Φ_1 tide are extremely large. The main reason for this behaviour is that these two waves have small amplitudes (3 mm and 5 mm, respectively) and lie close to the NDFW resonance. Extreme uncertainties in determining these two waves are also obtained by the evaluation of the real data (see Chapter Ch 4.4.2).

| | h_2 | l_2 | $h_{2l}(O_1)$ | $h_{2l}(P_1)$ | $h_{2l}(K_1)$ | $h_{2l}(\psi_1)$ | $h_{2l}(\Phi_1)$ | $h_{2l}(J_1)$ |
|--------------------|--------------|--------------|---------------|---------------|---------------|------------------|------------------|---------------|
| mean value | 0.6078 | 0.0847 | 0.6028 | 0.5817 | 0.5236 | 1.0569 | 0.6645 | 0.6108 |
| standard deviation | ± 0.0604 | ± 0.0222 | ± 0.2600 | ± 12.1187 | ± 4.5083 | ± 574.2080 | ± 280.9325 | ± 8.6703 |

Table (T 4.9): Love parameters with their standard deviations from the simulation.

Results from the “second” part of the program for h_{RS} and ω_{FCN} can be seen in Figures (F 4.21) and (F 4.22) or in the connected Tables (T 4.10) and (T 4.11), respectively. It follows, that five iterations were necessary.

The estimated value for $h_{2l}(O_1)$ is 0.6027, which differs from the input value 0.6028. This difference is due to the fit of the defining curve to only frequencies from five tides.

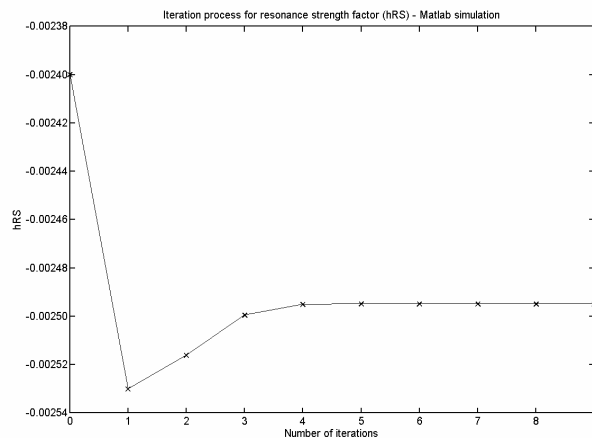
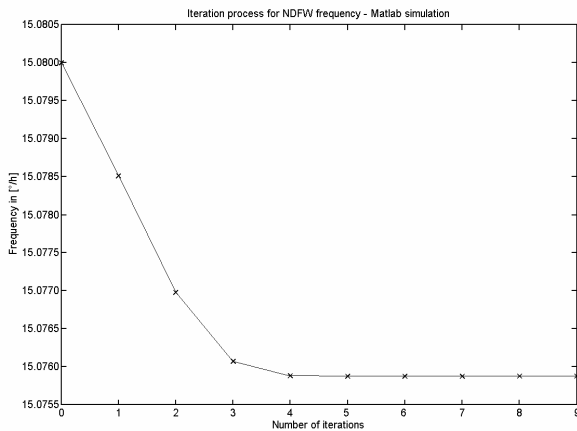


Figure (F 4.21): Iterative process for h_{RS} in Matlab simulation.

| i | h_{RS} |
|-----|--------------------|
| 0 | -0.00240000 |
| 1 | -0.00253013 |
| 2 | -0.00251613 |
| 3 | -0.00249957 |
| 4 | -0.00249503 |
| 5 | -0.00249496 |
| 6 | -0.00249496 |
| 7 | -0.00249496 |
| 8 | -0.00249496 |
| 9 | -0.00249496 |

Table (T 4.10): 9 iteration’s steps for h_{RS} .



| <i>i</i> | Frequency [°/h] |
|----------|--------------------|
| 0 | 15.08000000 |
| 1 | 15.07850975 |
| 2 | 15.07697917 |
| 3 | 15.07607088 |
| 4 | 15.07588370 |
| 5 | 15.07587747 |
| 6 | 15.07587746 |
| 7 | 15.07587746 |
| 8 | 15.07587746 |
| 9 | 15.07587746 |

Figure (F 4.22): Iterative process for NDFW frequency in Matlab simulation.

Table (T 4.11): 9 iteration's steps for ω_{FCN} .

4.3.4 Influence of inexact h_2 on radial displacement

To get an idea, how large the influence of a wrong Love number h_2 on the estimated site displacement is, see Figure (F 4.23). The displacement due to the second degree tidal potential was computed once with the correct Love number $h_2 = 0.6078$ and then with $h_2 = 0.5078$. As follows from the (F 4.23) the difference of 0.1 in the nominal Love number h_2 can cause a displacement error up to 6 cm (station HartRAO at 11 h UTC).

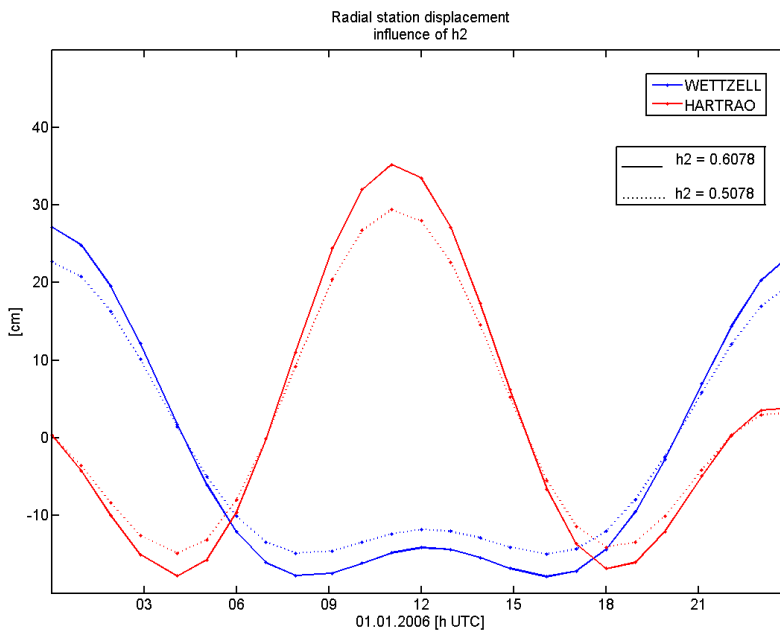


Figure (F 4.23): Influence of wrong second degree Love number ($h_{2_wrong} = 0.5078$; dotted line). The correct Love number $h_2 = 0.6078$ is plotted in solid line. The displacement error in radial direction reaches up to 6 cm.

4.4 Analysis in OCCAM

In OCCAM the model for solid Earth tides is coded in the program “matthew.f” and follows the currently recommended model from the IERS Conventions 2003. The theoretical computation procedure is described in detail in Chapter (Ch 1.4).

Partial derivatives of the tidal displacement with respect to the Love numbers h_2 , l_2 and to the six frequency dependent numbers $h_{2l}(O_1)$, $h_{2l}(P_1)$, $h_{2l}(K_1)$, $h_{2l}(\psi_1)$, $h_{2l}(\Phi_1)$, $h_{2l}(J_1)$ have been added. The code is described in Chapter (Ch 4.3.2). The essential equations are (E 4.3 – E 4.5) together with (E 1.30 – E 1.32).

The program allows to estimate from one VLBI session the Love numbers separately or together; however, only these combinations are possible:

$h_2&l_2$; $h_2&h_{2l}(f)$; $l_2&h_{2l}(f)$; $h_2&l_2&h_{2l}(f)$

i.e., only one frequency dependent Love number can be estimated at a time.

In this diploma thesis, the estimation of the frequency dependent numbers is considered only as a first attempt to determine these values. From one-day sessions it is very problematic to obtain realistic values, and therefore in the future it will be necessary to estimate $h_{2l}(f)$ from a global VLBI solution involving a large time span of several years. This is the reason, why I did not estimate more frequency dependent values.

The main settings of the software for the VLBI data analysis were as follows:

- Catalogue of the radio sources: ITRF2005.G27
- Cut off elevation angle: 5.0°
- No estimation of source coordinates

4.4.1 Nominal values h_2 and l_2

| Deviations from theoretical value $h_2 = 0.6078$ | | | | | | |
|--|-----------------|----------------|---------------------|----------------|-----------------------------------|----------------|
| Datum | All 11 stations | | | | 10 stations (without TIGOCONC) | |
| | l_2 estimated | | l_2 not estimated | | l_2 estimated | |
| | free net | fix net | free net | fix net | free net | fix net |
| 05-09-12 | 0.0142 | -0.0074 | 0.0197 | -0.0019 | 0.0153 | -0.0073 |
| 05-09-13 | 0.0296 | 0.0112 | 0.0204 | 0.0015 | 0.0288 | 0.0110 |
| 05-09-14 | 0.0299 | -0.0149 | 0.0304 | -0.0120 | 0.0248 | -0.0115 |
| 05-09-15 | -0.0125 | -0.0328 | -0.0072 | -0.0266 | -0.0185 | -0.0376 |
| 05-09-16 | -0.0200 | -0.0555 | -0.0195 | -0.0548 | -0.0216 | -0.0592 |
| 05-09-17 | -0.0208 | -0.0336 | -0.0197 | -0.0300 | -0.0176 | -0.0317 |
| 05-09-18 | 0.0048 | -0.0265 | 0.0048 | -0.0268 | 0.0112 | -0.0236 |
| 05-09-19 | 0.0118 | -0.0252 | 0.0121 | -0.0212 | 0.0071 | -0.0287 |
| 05-09-20 | 0.0352 | -0.0034 | 0.0365 | 0.0006 | 0.0304 | -0.0061 |
| 05-09-21 | 0.0002 | -0.0159 | 0.0009 | -0.0148 | 0.0017 | -0.0151 |
| 05-09-22 | 0.0096 | -0.0143 | 0.0091 | -0.0166 | 0.0145 | -0.0151 |
| 05-09-23 | 0.0041 | -0.0303 | 0.0039 | -0.0290 | 0.0001 | -0.0323 |
| 05-09-24 | 0.0338 | 0.0111 | 0.0277 | 0.0030 | 0.0357 | 0.0103 |
| 05-09-25 | 0.0130 | -0.0225 | 0.0240 | -0.0161 | 0.0117 | -0.0251 |
| 05-09-26 | 0.0270 | -0.0083 | 0.0294 | 0.0038 | 0.0278 | -0.0093 |
| mean value | 0.0106 | -0.0179 | 0.0115 | -0.0161 | 0.0101 | -0.0188 |
| standard deviation | ±0.0070 | ±0.0058 | ±0.0068 | ±0.0055 | ±0.0071 | ±0.0058 |

Table (T 4.12): Deviations from nominal Love number h_2 estimated from CONT05 campaign.

Several configurations in the computational approach were applied. The first set of values in Table (T 4.12) and Table (T 4.13) refers to the free network solution, where the station coordinates were estimated with an NNR/NNT condition (no net rotation / not net translation). In the second column are the results obtained from data evaluation with fixed station coordinates. In both columns, both Love numbers (h_2 and l_2) were estimated. The following two columns refer again to a free network and fixed network, respectively; however in this case only the Love number h_2 was determined.

As one can see, the differences between the values obtained from the fixed network (green lines in Figures (F 4.24 and F 4.25)) and from the free solution (black lines) are shifted by an offset of about 0.02 for Love number h_2 . For the Shida number l_2 the values are about the same.

Focusing on the solid and dashed lines in Figures (F 4.24 and F 4.25) it follows, that a simultaneous estimation of the Love numbers and a separate estimation of h_2 or l_2 , causes no significant difference in the obtained values.

Because of the big differences between the values from individual sessions, there was an idea (due to previous experience) to exclude the station TIGOCONC from the experiment, hoping to obtain less variable results. However, this hypothesis was not confirmed. As can be seen in the last two columns of tables (T 4.12) and (T 4.13) and in Figure (F 4.26) for h_2 , no improvement concerning the spread in the estimated Love numbers was obtained.

| Deviations from theoretical value $l_2 = 0.0847$ | | | | | | |
|--|-----------------|----------------|---------------------|----------------|-----------------------------------|----------------|
| Datum | All 11 stations | | | | 10 stations (without TIGOCONC) | |
| | h_2 estimated | | h_2 not estimated | | h_2 estimated | |
| | free net | fix net | free net | fix net | free net | fix net |
| 05-09-12 | -0.0024 | -0.0023 | -0.0030 | -0.0019 | -0.0022 | -0.0025 |
| 05-09-13 | 0.0054 | 0.0052 | 0.0045 | 0.0048 | 0.0053 | 0.0051 |
| 05-09-14 | -0.0010 | -0.0018 | -0.0019 | -0.0014 | -0.0009 | -0.0016 |
| 05-09-15 | -0.0036 | -0.0037 | -0.0034 | -0.0028 | -0.0040 | -0.0040 |
| 05-09-16 | -0.0012 | -0.0007 | -0.0011 | 0.0002 | -0.0016 | -0.0012 |
| 05-09-17 | -0.0027 | -0.0028 | -0.0027 | -0.0022 | -0.0027 | -0.0028 |
| 05-09-18 | 0.0001 | 0.0003 | 0.0002 | 0.0006 | -0.0002 | 0.0001 |
| 05-09-19 | -0.0044 | -0.0034 | -0.0044 | -0.0030 | -0.0045 | -0.0035 |
| 05-09-20 | -0.0037 | -0.0030 | -0.0038 | -0.0029 | -0.0041 | -0.0032 |
| 05-09-21 | -0.0007 | -0.0008 | -0.0007 | -0.0003 | -0.0011 | -0.0010 |
| 05-09-22 | 0.0003 | 0.0012 | 0.0001 | 0.0019 | 0.0007 | 0.0012 |
| 05-09-23 | 0.0001 | -0.0005 | -0.0001 | 0.0010 | -0.0014 | -0.0014 |
| 05-09-24 | 0.0028 | 0.0034 | 0.0008 | 0.0026 | 0.0034 | 0.0032 |
| 05-09-25 | -0.0050 | -0.0027 | -0.0058 | -0.0010 | -0.0052 | -0.0032 |
| 05-09-26 | -0.0014 | -0.0030 | -0.0024 | -0.0026 | -0.0019 | -0.0034 |
| mean value | -0.0024 | -0.0023 | -0.0030 | -0.0019 | -0.0022 | -0.0025 |
| standard deviation | ±0.0009 | ±0.0008 | ±0.0009 | ±0.0008 | ±0.0009 | ±0.0009 |

Table (T 4.13): Deviations from nominal Shida number l_2 estimated from CONT05 campaign.

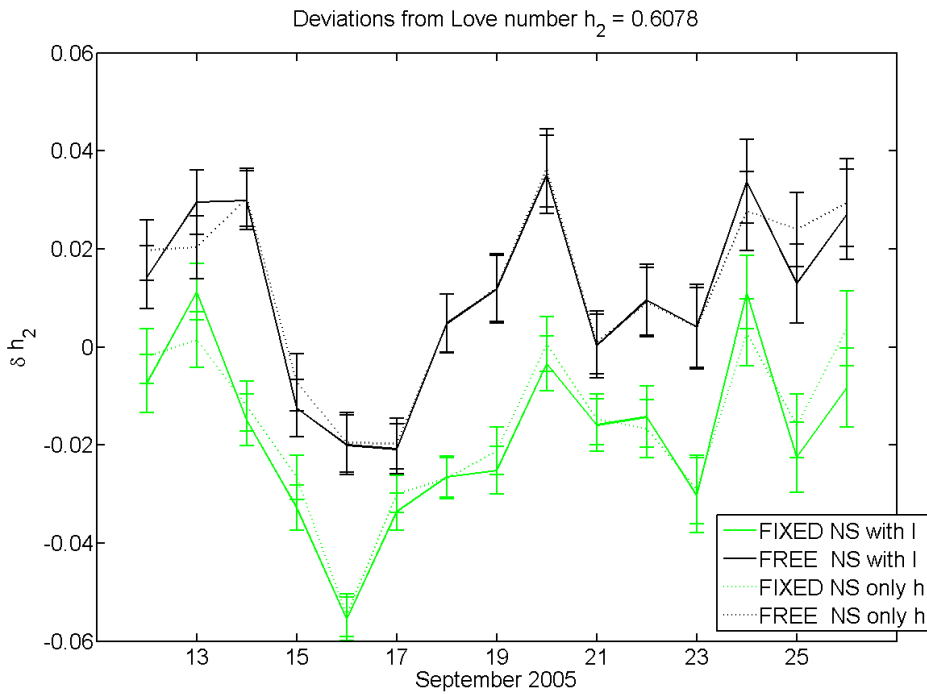


Figure (F 4.24): Deviations from nominal Love number h_2 estimated from CONT05 campaign. Green and black lines show the values obtained from fixed and free network, respectively. Results from approach, where Shida number l_2 was simultaneous estimated are plotted in solid lines, whereas the dotted lines stay for separate h_2 estimation.

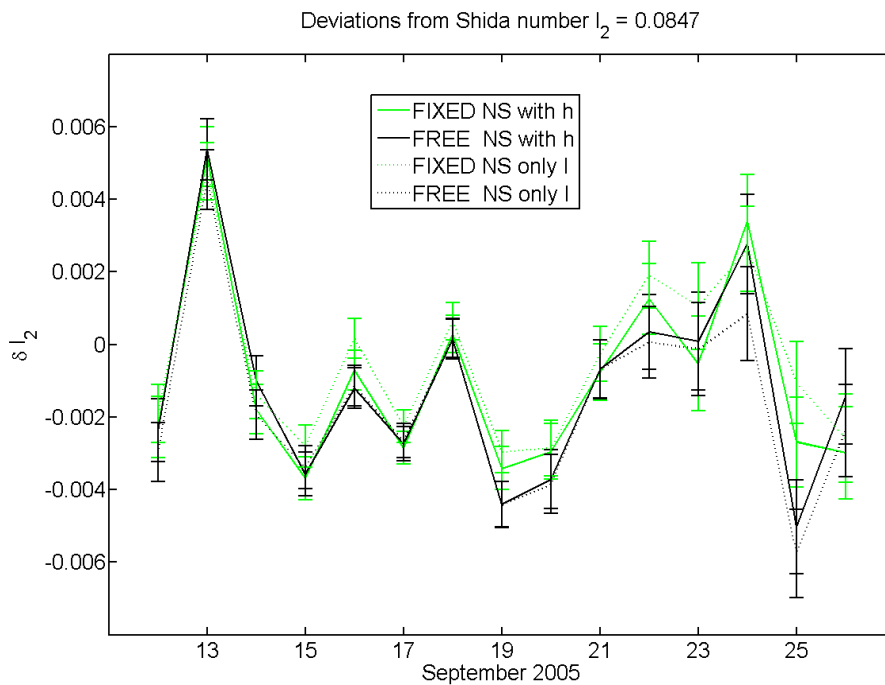


Figure (F 4.25): Deviations from nominal Shida number l_2 estimated from CONT05 campaign. Green and black lines show the values obtained from fixed and free network, respectively. Results from approach, where Love number h_2 was simultaneous estimated are plotted in solid lines, whereas the dotted lines stay for separate l_2 estimation.

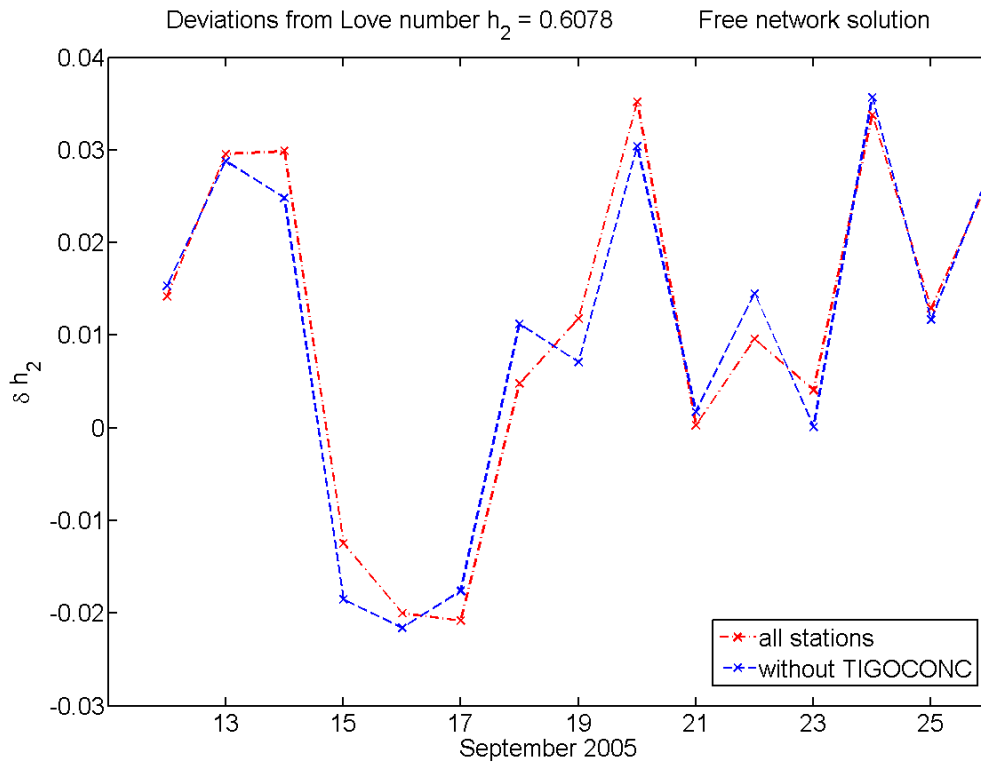


Figure (F 4.26): Comparison between δh_2 estimated from measurements at all stations participated in CONT05 campaign (red line) and at only 10 stations – without TIGOCONC (blue line).

| mean values of estimated theoretical Love numbers: $h_2 = 0.6078$ $l_2 = 0.0847$ | | | | | | |
|--|---|--------------|--|--------------|---|--------------|
| Datum | All 11 stations | | | | 10 stations (without TIGOCONC) | |
| | parallel estimation of h_2 and l_2 | | separate estimation of h_2 or l_2 | | parallel estimation of h_2 and l_2 | |
| | free net | fix net | free net | fix net | free net | fix net |
| h_2 | 0.6184 | 0.5899 | 0.6193 | 0.5917 | 0.6179 | 0.5890 |
| standard deviation | ± 0.0070 | ± 0.0058 | ± 0.0068 | ± 0.0055 | ± 0.0071 | ± 0.0058 |
| l_2 | 0.0823 | 0.0824 | 0.0817 | 0.0828 | 0.0825 | 0.0822 |
| standard deviation | ± 0.0009 | ± 0.0008 | ± 0.0009 | ± 0.0008 | ± 0.0009 | ± 0.0009 |

Table (T 4.14): Mean values of Love numbers h_2 and l_2 estimated from CONT05 campaign.

4.4.2 Frequency dependent h_{21} for six diurnal waves

| Tide | Argument number | Love number $h_{21}(f)$ | | |
|----------|-----------------|-------------------------|------------------------|--------------------|
| | | (IERS Conventions 2003) | (Haas and Schuh, 1996) | This thesis |
| O_1 | 145.555 | 0.6028 | 0.560 ± 0.012 | 0.631 ± 0.016 |
| P_1 | 163.555 | 0.5817 | 0.574 ± 0.005 | 0.578 ± 0.036 |
| K_1 | 165.555 | 0.5236 | 0.496 ± 0.002 | 0.537 ± 0.012 |
| ψ_1 | 166.554 | 1.0569 | -0.136 ± 0.228 | -1.484 ± 1.459 |
| Φ_1 | 167.555 | 0.6645 | 0.702 ± 0.121 | 1.559 ± 0.879 |
| J_1 | 175.455 | 0.6108 | 0.538 ± 0.031 | 1.039 ± 0.250 |

Table (T 4.15): Estimates of frequency dependent $h_{21}(f)$, see (F 4.33).

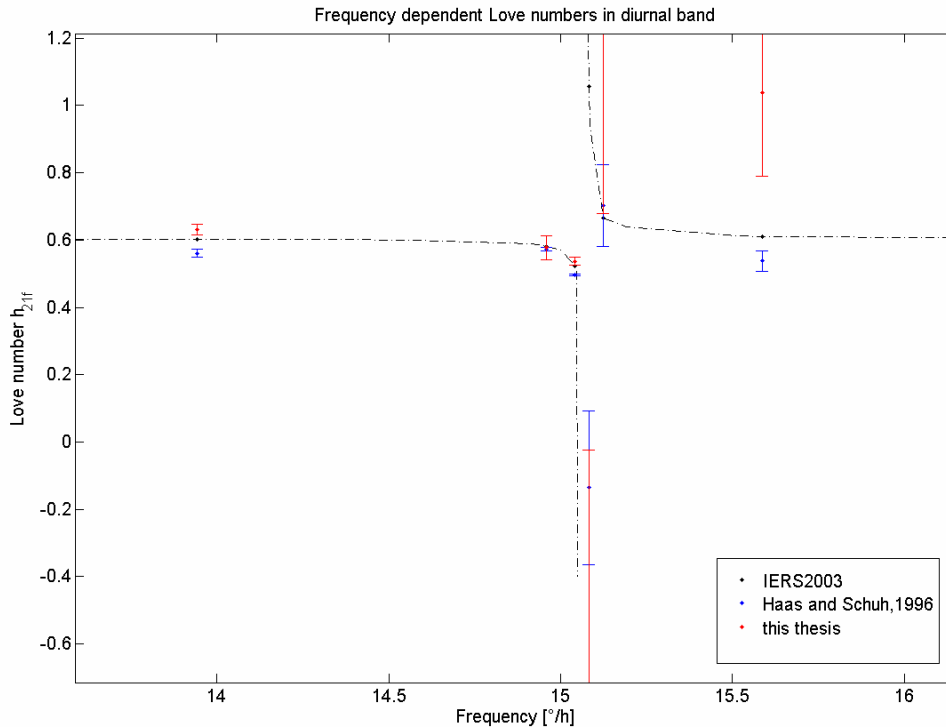


Figure (F 4.33): Estimates of frequency dependent Love numbers in diurnal band $h_{21}(f)$. The frequency of NDFW was fixed.

Figure (F 4.33) shows the mean estimated value of frequency dependent Love numbers in diurnal band from the CONT05 campaign (red ones). It is compared with results achieved by Haas and Schuh (1996) plotted in blue lines. The black dotted line interpolates between currently adopted Love number values (McCarthy and Petit, 2004) from diurnal band. The frequency of NDFW was fixed. It is evident, that the values from the weak tides close to the resonance become larger and their formal errors are huge. It is interesting that a similar shift

of $h_{2l}(\psi_1)$ is found here which has already been reported by Haas and Schuh (1996). The estimated value is on the other part of the resonance curve. The “official value” is 1.0569, whereas the results of Haas and Schuh (1996) and this thesis provide a negative values of -0.136 ± 0.228 and -1.484 ± 1.459 , respectively. However, it should be paid attention to the enormous standard deviation making my result uncertain.

The weak J1 tide also does not correspond to its expected value. The reason should be in the low amplitude and the time span, which is not adequate for its estimation.

On the other hand, one can see agreeing results for the three strong tides: K_1 , O_1 , P_1 . They are close to their theoretical values and the difference is less than twice the standard deviation.

In the following six figures (F 4.27 – F 4.32) the sequence of the estimated values for each tide is plotted as derived from 24-hours VLBI – sessions from the period 12th – 26th September 2006.

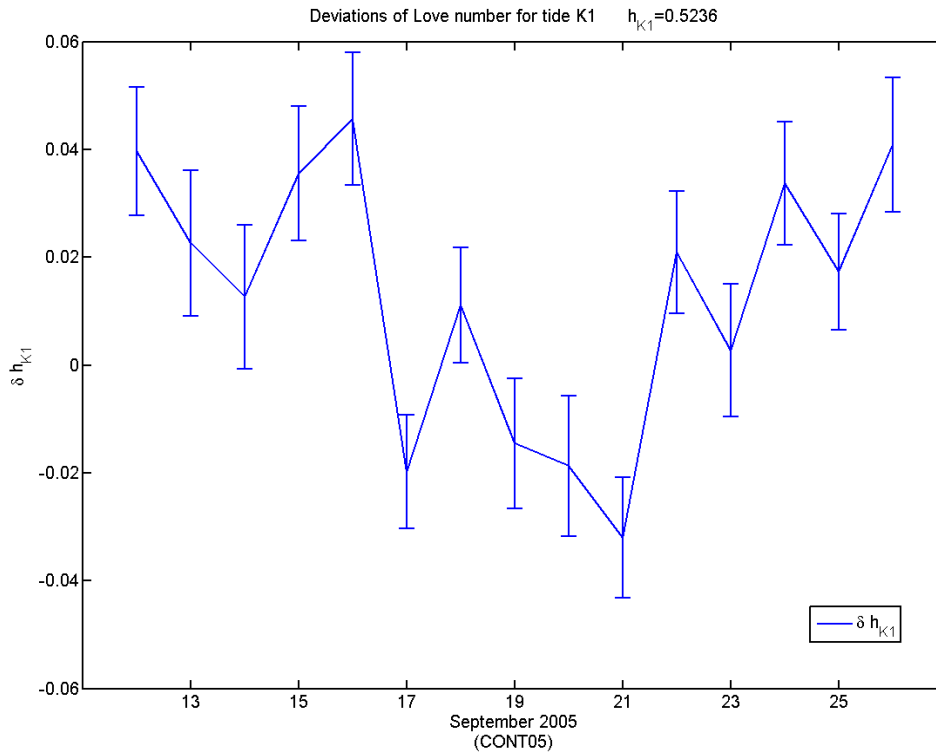


Figure (F 4.27): Deviations of $h_{2l}(K_1)$ from the value defined in IERS2003.

$$\delta h_{2l}(K_1) = 0.013 \pm 0.012$$

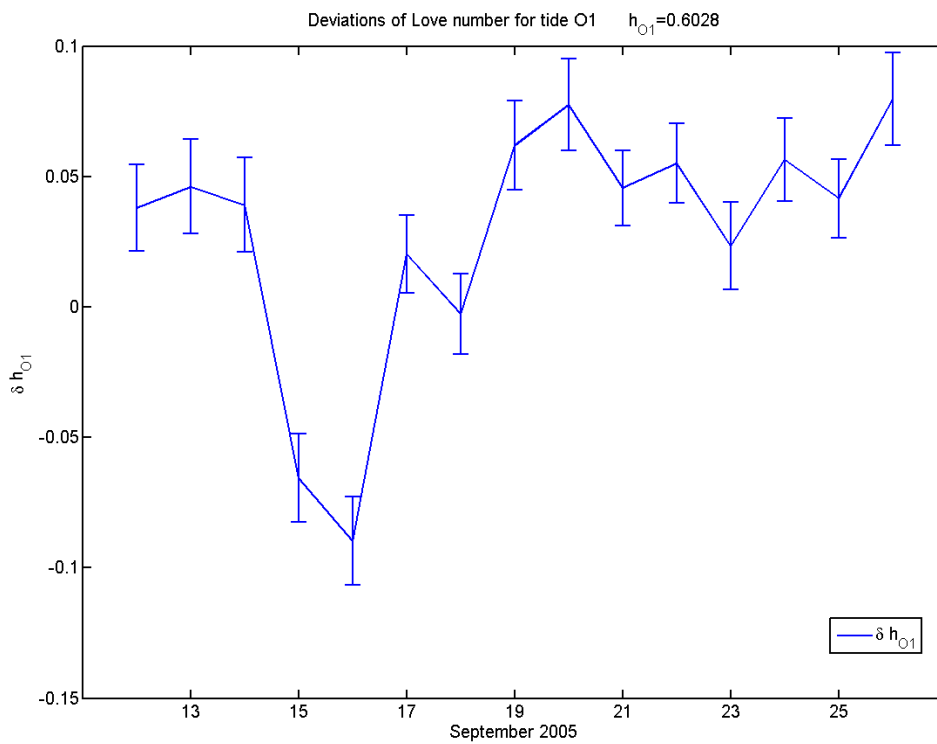


Figure (F 4.28): Deviations of $h_{2l}(O_1)$ from the value defined in IERS2003.

$$\delta h_{2l}(O_1) = 0.028 \pm 0.016$$

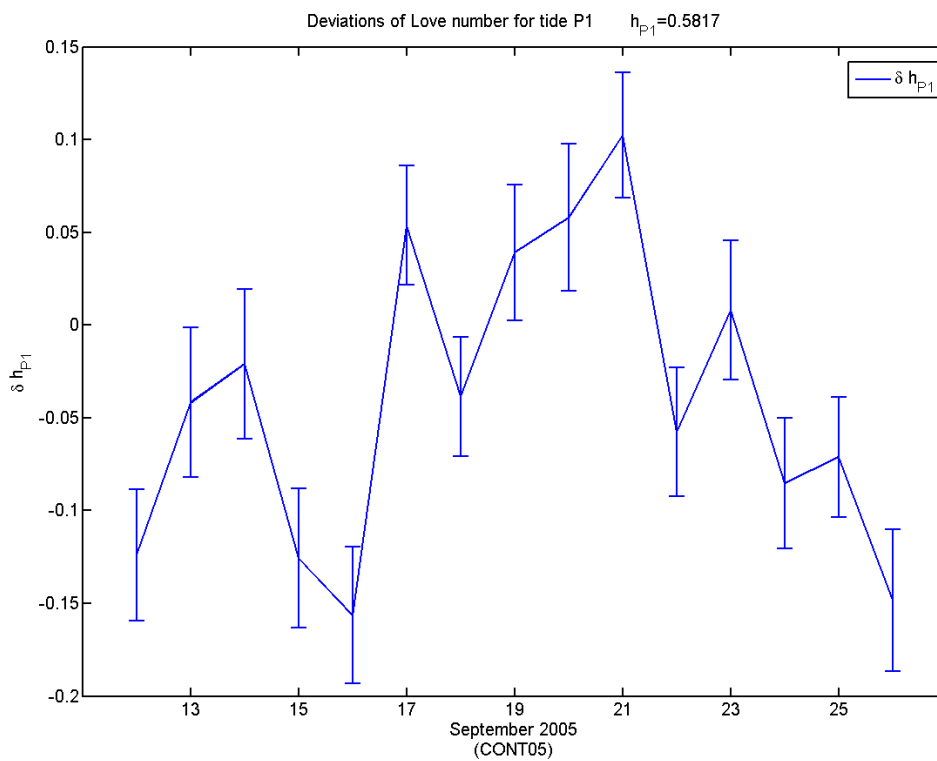


Figure (F 4.29): Deviations of $h_{2l}(P_1)$ from the value defined in IERS2003.

$$\delta h_{2l}(P_1) = -0.004 \pm 0.036$$

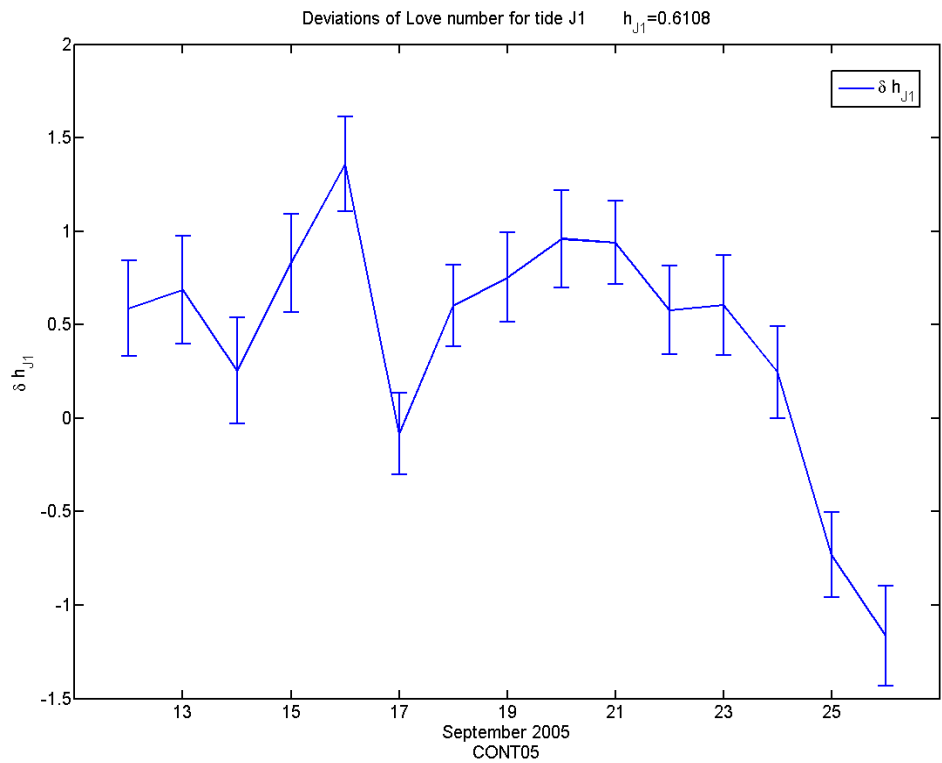


Figure (F 4.30): Deviations of $h_{2l}(J_1)$ from the value defined in IERS2003.

$$\delta h_{2l}(J_1) = 0.428 \pm 0.250$$

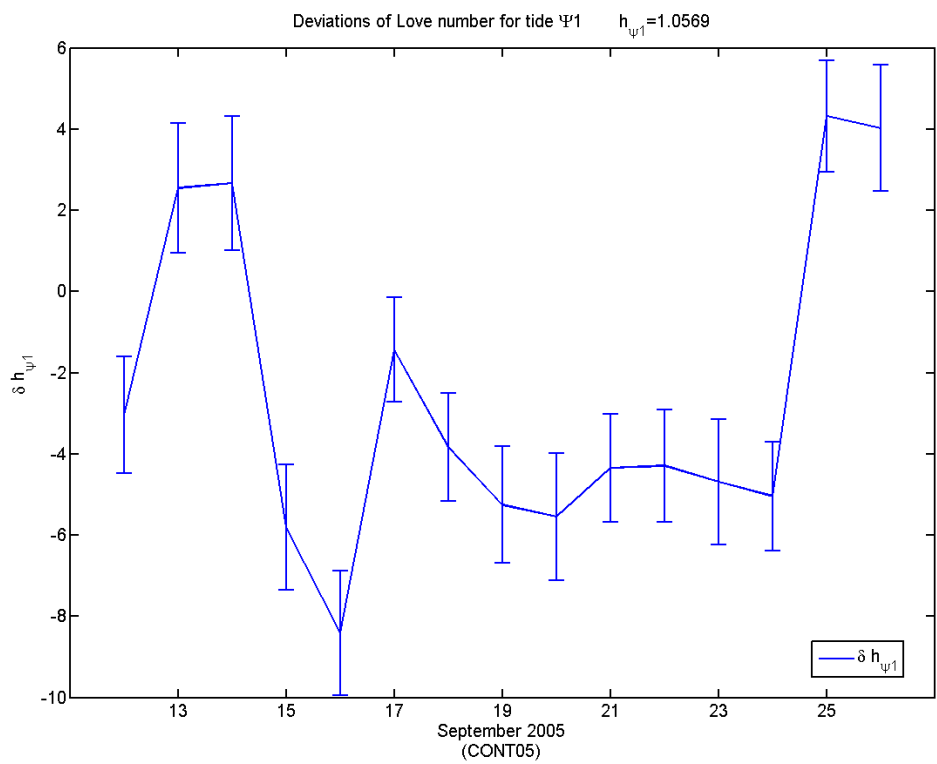


Figure (F 4.31): Deviations of $h_{2l}(\psi_1)$ from the value defined in IERS2003.

$$\delta h_{2l}(\psi_1) = -2.541 \pm 1.459$$

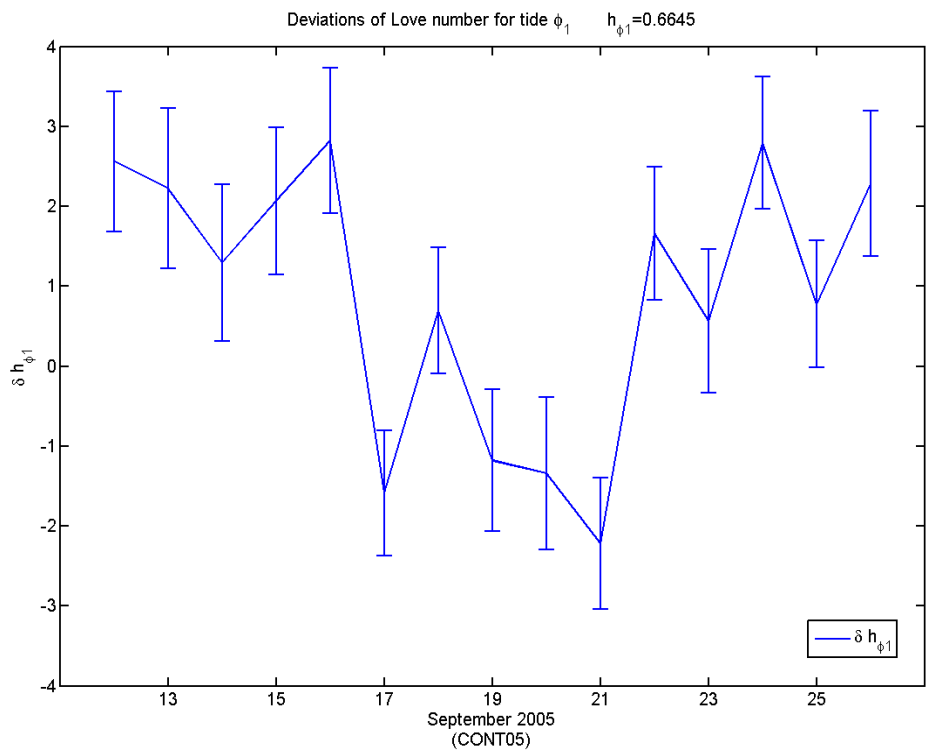


Figure (F 4.32): Deviations of $h_{2l}(\Phi_1)$ from the value defined in IERS2003.

$$\delta h_{2l}(\Phi_1) = 0.8945 \pm 0.879$$

5. Conclusions

Second degree Love and Shida numbers of the solid Earth tide model were determined from 24-hour VLBI sessions of the CONT05 campaign.

Considering the Earth being spherical, non-rotating, elastic and isotropic, the Love numbers on the Earth's surface are dependent only on the degree of the tide generating potential. The estimated value corresponding to h_2 is 0.618 ± 0.007 , which differs by 0.011 from its theoretical value. The estimate for the Shida number l_2 is 0.082 ± 0.001 with a difference of about -0.002 from its theoretical value. Better results with respect to the predicted values were found with a free network solution instead of fixed station coordinates.

One possible reason for the larger differences in the h_2 estimates is its dependence on the displacement in radial direction. The radial component (i.e. the differences in height of the station) is often subject to errors caused, e.g., from the signal's travel through the atmosphere or from approaches, which do not correct disturbing influences on VLBI measurements precisely enough, e.g., atmosphere and ocean loading corrections.

The determination of frequency dependent Love numbers, which arise under the assumption of a rotating Earth, was rather an attempt to see if any reasonable values from 24-hour sessions can be obtained than a rigorous determination. Sufficient results were achieved for the tides K_1 , O_1 , P_1 with large amplitudes for which the estimated values differ from the theoretical values by less than twice their standard deviation. For the three weak tides J_1 , ψ_1 , Φ_1 close to the NDFW resonance the obtained values are "insignificant" with respect to their large standard deviations. The improvement in the determination of these tides will be based on the extension of the time span of VLBI sessions. In other words, these tides need to be estimated within a global VLBI solution over at least several years.

References

- Brosche, P., Schuh, H.: *Neue Entwicklungen in der Astronomie und Bedeutung für die Geodäsie*. ZfV 11/1999.
- Burša, M., Kostecký, J.: *Space geodesy and space geodynamics*. Ministry of Defense. Prague 1999.
- Burša, M., Pěč, K.: *Tíhové pole a dynamika Země*. Academia. Praha 1988.
- Campbell, J., Nothnagel, A., Schuh, H.: *Die Radiointerferometrie auf langen Basislinien (VLBI) als geodätisches Meßverfahren höchster Genauigkeit*. Allgemeine Vermessungsnachrichten. Vol. 11-12/1992.
- Campbell, J.: *VLBI for Geodesy and Geodynamics*. In: F. Mantovani and A. Kus (Eds): *The Role of VLBI in Astrophysics, Astrometry and Geodesy*. Kluwer Academic Publishers. 2004. p. 359-381.
- Cartwright, D.E., Tayler, R.J.: *New computations of the tide-generating potential*. Geophys. J. Roy. Astron. Soc.. Vol 23/1971. p. 45–74.
- Haas, R., Schuh, H.: *Determination of frequency dependent Love and Shida numbers from VLBI data*. Geophysical Research Letters. Vol. 23 No.12/1996. p. 1509-1512.
- IERS Conventions (2003)*. Dennis D., McCarthy and Gérard Petit. (IERS Technical Note; 32) Frankfurt am Main: Verlag des Bundesamts für Kartographie und Geodäsie. 2004. paperback. ISBN 3-89888-884-3 (print version).
- Mathews, P.M., Buffett B.A., Shapiro I.I.: *Love numbers for a rotating spheroidal Earth: New definition and numerical values*. Geophysical Research Letters. Vol.22 No.5/1995.
- Mathews, P.M., Dehant V., Gipson J.M.: *Tidal station displacements*. Journal of Geophysical Research. Vol.102 No.B9/1997.
- Melchior, P.: *The tides of the Planet Earth*. Pergamon Press. Oxford 1983. Second edition.
- Love, A.E.H.: *Treatise on the mathematical theory of elasticity*. Cambridge 1927. Fourth edition.
- Schlüter, W., Behrend, D.: *The International VLBI Service for Geodesy and Astrometry (IVS): current capabilities and future prospects*. Journal of Geodesy. Vol. 81 No. 6-8/2007. p. 379-387(9).
- Schuh, H.: *Contributions of VLBI to Space Geodesy*. In: Rummel, R., Drewes, H., Bosch, W., Hornik, H. (Eds): *Proceedings of the international symposium 'Towards an Integrated Global Geodetic Observing System'*. Munich 1998. Springer IAG Symposia series. Vol. 120/2000. p. 33-40.

Schuh, H. et al.: *IVS Working Group 2 for Product Specification and Observing Programs, Final Report* (13th of February 2002).

http://ivscc.gsfc.nasa.gov/about/wg/wg2/IVS_WG2_report_130202.pdf

Sovers, O.J., J.L. Fanselow, & C.S. Jacobs. *Astrometry & Geodesy with Radio Interferometry: Experiments, Models, Results*. Rev. Mod. Phys.. Vol. 70 No. 4/1998. p. 1393-1454.

Vondrák, J., Ron, C.: *Resonant period of Free Core Nutation – Its observed changes and excitations*. Acta Geodyn. Geomater.. Vol. 3 No. 3/2006 p. 53-60.

Wahr, J.: *Earth Tides*. In: T.J. Ahrens (Eds): *Global earth physics a handbook of physical constants*. Publisher: Washington, DC American Geophysical Union. 1995. p. 40-46.

Weber, R.: *Theorie des Erdschwerefeldes*. Class Notes, TU Vienna 2007.

Zeman, A.: *Fyzikální geodézie*. Vydavatelství ČVUT. Praha 2005.

Zürn, W.: *The Nearly-Diurnal Free Wobble-Resonance*. In: Wilhelm H., Zürn W., Wenzel H.: *Tidal phenomena*. Springer Verlag. 1997. p. 95-107.

Weblinks

proof of the links: 2008-04-27

Agnew, D.C.: *Earth Tides: An Introduction*.

<http://www.unavco.org:8080/cws/straindata/Notesfrom2005class/tidenote.pdf>.

Titov, O., Tesmer, V., Boehm, J.: *OCCAM v. 6.0 software for VLBI data analysis*. 2004.

ftp://ftp.ga.gov.au/sgac/vlbi/OCCAM6_0/DOC/occam.pdf

Schuh, H.: *OCCAM – A modern VLBI Software Package with a long History*.

[1] http://ivs.nict.go.jp/mirror/analysis/Schuh_OCCAM5.0_Preface.doc

